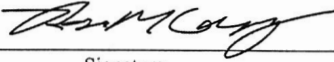
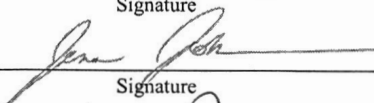
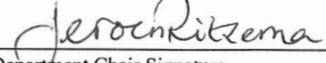


Nathan LaFramboise

Controls on the photochemical production of hydrogen peroxide in arctic surface waters

submitted in partial fulfillment of the requirements for the degree of
Master of Science in Earth and Environmental Sciences
Department of Earth and Environmental Sciences
The University of Michigan

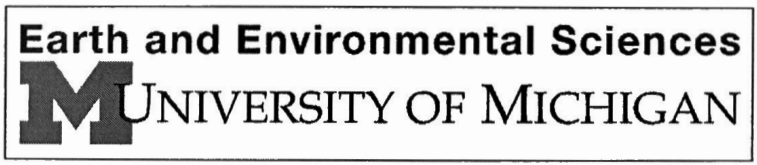
 _____ Signature	Accepted by: Rose Cory _____ Name	4-April-2024 _____ Date
 _____ Signature	Jena E. Johnson _____ Name	4/4/2024 _____ Date
 _____ Department Chair Signature	JEROEN RITSEMA _____ Name	4/4/2024 _____ Date

I hereby grant the University of Michigan, its heirs and assigns, the non-exclusive right to reproduce and distribute single copies of my thesis, in whole or in part, in any format. I represent and warrant to the University of Michigan that the thesis is an original work, does not infringe or violate any rights of others, and that I make these grants as the sole owner of the rights to my thesis. I understand that I will not receive royalties for any reproduction of this thesis.

- Permission granted.
- Permission granted to copy after: _____
- Permission declined.



Author Signature



Abstract

Photochemical production of hydrogen peroxide (H_2O_2) from chromophoric/colored dissolved organic matter (CDOM) is a major source of H_2O_2 in natural waters. In a rapidly warming Arctic, H_2O_2 may increase due to thawing permafrost soils that are expected to export more CDOM to sunlit surface waters. At the same time, arctic surface waters are increasingly ice-free and thus exposed to sunlight for greater lengths of time during the summer. Thus, it has been hypothesized that photochemical production of H_2O_2 and H_2O_2 concentrations may increase in arctic surface waters. Testing this hypothesis requires determination of whether H_2O_2 production by CDOM is limited by CDOM concentration (substrate-limited) or by sunlight (light-limited). In waters with high concentrations of CDOM, H_2O_2 production may be limited by the sunlight reaching the water. In waters with low concentrations of CDOM, H_2O_2 production may be limited by CDOM concentration. This study quantified the substrate and light limitation of H_2O_2 production in surface waters of the Alaskan Arctic in summer 2022 and 2023. In each water, concentrations of CDOM were measured along with the apparent quantum yield of H_2O_2 ($\phi_{\text{H}_2\text{O}_2,\lambda}$) produced from CDOM. The $\phi_{\text{H}_2\text{O}_2,\lambda}$ increased with increasing aromatic content of the CDOM. Photochemical production rates for all waters in this study were strongly limited by sunlight and limited by CDOM concentration. Photochemical production of H_2O_2 increased linearly with increasing sunlight and non-linearly with increasing CDOM. Thus, increasing sunlight exposure of arctic lakes (due to less ice cover) will increase H_2O_2 production and likely increase H_2O_2 concentrations. Likewise, increasing CDOM concentrations in arctic lakes due to export of CDOM from thawing permafrost soils will likely also increase H_2O_2 production in lake waters where H_2O_2 production is limited by CDOM.

List of relevant acronyms:

H₂O₂: Hydrogen peroxide

ROS: Reactive oxygen species

DOM: Dissolved organic matter

DOC: Dissolved organic carbon

CDOM: Chromophoric (light-absorbing) dissolved organic matter

$\phi_{\text{H}_2\text{O}_2,\lambda}$: Apparent quantum yield of hydrogen peroxide production from CDOM

PH₂O₂: Photochemical production of hydrogen peroxide

·OH: Hydroxyl Radical

Fe: Dissolved iron

***a*X (305, CDOM, TOT, etc)**: The absorbance of something – italicized as is convention for the field of photochemistry

[H₂O₂]_{ss}: Steady state concentration of hydrogen peroxide

1. Introduction

Hydrogen peroxide (H₂O₂) is a reactive oxygen species (ROS) produced in all natural waters on Earth, where it acts as an oxidative stressor and influences redox cycling of carbon and trace metals (Cooper et al., 1994; Lesser, 2006; Moffett & Zika 1987). Chromophoric fractions of dissolved organic matter produce H₂O₂ by the absorption of ultraviolet (UV) sunlight (CDOM; Cooper et al., 1994; Petasne & Zika 1987; Scully et al., 1996). Absorption of light by CDOM initiates the excited state CDOM*, which facilitates excited-state electron transfer processes that reduce dissolved oxygen (O₂) to superoxide (O₂⁻), which further undergoes dismutation to produce H₂O₂ (Zhang et al., 2012).

Briefly, the history of research on H₂O₂ has been centered around its role as an oxidative stressor and influencer of trace metal cycling. Production and decay of H₂O₂ is a major focus of the current research and controls on these dynamics are not well understood in surface waters. Biological production and decay, photochemical production, and abiotic decay of H₂O₂ all influence the steady state concentration of H₂O₂ in surface waters ([H₂O₂]_{ss}). Understanding what controls the production and decay of H₂O₂ leads to better understanding of how H₂O₂ influences biogeochemical cycles in surface waters (eg. oxidative stress, metal cycling). The goal of this study was to provide a foundational understanding for H₂O₂ in arctic surface waters, where it has never been quantified. The work for this study was conducted at Toolik Field Station in the Alaskan Arctic, where arctic research has been conducted for 50 years. This work is affiliated with the Arctic Long Term Ecological Research Network (Arctic LTER), which has been operating at Toolik Field Station since its inception.

Arctic surface waters have high concentrations of dissolved organic matter (DOM), and CDOM, respectively (Cory et al., 2007; Gareis et al., 2010). These waters are also unshaded and shallow, which are often exposed to sunlight throughout the entire water column. Thus, it has been hypothesized that arctic surface waters are high in concentrations of H₂O₂ (Cory et al., 2010). However, no study has quantified H₂O₂ in arctic surface waters.

The role of H₂O₂ as an oxidative stressor may have important implications for the arctic carbon cycle. One major pathway of dissolved organic carbon (DOC) processing in arctic surface waters is through microbial respiration and sunlight-stimulated microbial respiration of DOC to CO₂ (Cole et al., 1994; Cory et al., 2014; Kling et al., 1991). Oxidative stress from H₂O₂ may impact microbial communities facilitating the release of CO₂ from arctic surface waters from DOC. Thus, understanding the role of H₂O₂ on these microbial communities is critical for quantifying CO₂ production from the coupled photochemical and microbial degradation of DOC (Cory et al., 2014; Ward et al., 2017). Furthermore, in lower latitude freshwaters, evidence suggests that H₂O₂ influences microbial community composition and leads to the formation of cyanobacterial toxic algal blooms (Cory et al., 2016; Hellweger et al. 2022). The proportion of cyanobacteria in microbial communities in Toolik Lake, Alaska has increased over the past 20 years (Natasha Christman PhD thesis *in prep*). Increasing proportions of cyanobacteria and high potential for H₂O₂ production in arctic surface waters demonstrates the need to quantify H₂O₂ production in these waters.

Rates of photochemical production of H₂O₂ (PH₂O₂) from CDOM are a product of two wavelength dependent spectra: 1) the apparent quantum yield spectrum of H₂O₂ produced from CDOM ($\phi_{\text{H}_2\text{O}_2,\lambda}$), which is represented by the amount of moles of H₂O₂ produced per mole of photons absorbed by CDOM as a function of wavelength (Kieber et al., 2014; Pandey et al., 2022), and 2) the amount of light absorbed from the photon flux by CDOM over the depth of the water column. The latter is well understood in arctic surface waters (Cory et al., 2014; Cory et al., 2015), but the $\phi_{\text{H}_2\text{O}_2,\lambda}$ in arctic surface waters is not known. Most prior work of $\phi_{\text{H}_2\text{O}_2,\lambda}$ in surface waters was conducted primarily in seawater (Andrews et al., 2000; Kieber et al., 2014; O'Sullivan et al., 2005; Powers & Miller, 2014). Only a few studies have reported lower latitude freshwater values of $\phi_{\text{H}_2\text{O}_2,\lambda}$ (Andrews et al., 2000; Cory et al., 2016; Pandey et al., 2022). Previous work suggested that the $\phi_{\text{H}_2\text{O}_2,\lambda}$ may depend strongly on the proportion of terrestrially derived DOM (O'Sullivan et al., 2005; Pandey et al., 2022; Powers & Miller, 2014). Arctic freshwaters characterized by high proportions of terrestrially-derived DOM (Whalen & Cornwell, 1985) may have high $\phi_{\text{H}_2\text{O}_2,\lambda}$ compared to lower latitude freshwaters and seawater.

The close coupling of H₂O₂ and dissolved iron (Fe) in surface waters via Photo-Fenton chemistry is well-documented (Haber et al., 1934.; J H Festos, 1894.; Stumm & Lee 1961.; Vermilyea & Voelker, 2009; Zepp et al., 1992). For example, in sunlit waters, H₂O₂ may oxidize Fe (II) and produce Fe (III) and hydroxyl radical ($\cdot\text{OH}$). Previous work suggested evidence that formation of $\cdot\text{OH}$ is closely related to dissolved iron in arctic surface waters (Page et al., 2014). Thus, Photo-Fenton chemistry is expected to occur rapidly in high iron arctic surface waters (Hammerschmidt & Fitzgerald, 2010; Page et al., 2014). Given the dependence of OH \cdot formation on dissolved iron (Page et al., 2014), the $\phi_{\text{H}_2\text{O}_2,\lambda}$ may depend strongly on dissolved iron. However, due to the known interference of dissolved iron on acridinium ester chemiluminescence flow-injection (FeLume) methods of measuring H₂O₂ (Cooper et al., 2000; King et al., 2007), we excluded waters with expected dissolved iron concentrations greater than 5 μM from this study. As a result, predictions of PH₂O₂ and [H₂O₂] in this study may be underestimated by biases in sample selection.

Constraining how the $\phi_{\text{H}_2\text{O}_2,\lambda}$ varies in arctic surface waters may inform understandings on the controls of the rates of PH₂O₂ in arctic surface waters. Arctic surface waters are becoming

increasingly ice-free, (Šmejkalová et al., 2016) thus lengthening surface waters exposure to sunlight. Longer exposure to sunlight may increase PH_2O_2 or increase the exposure of microbes to H_2O_2 over more days compared to the past where lakes were ice-covered for longer.

Beyond the Arctic, understanding the controls on PH_2O_2 in surface waters is important given the increase in CDOM concentrations in North American and European surface waters (De Wit et al., 2021; Monteith et al., 2007; Williamson et al., 2015). With increasing CDOM concentrations, it is expected that PH_2O_2 will also increase (Wolf et al., 2017, 2018). Thus, the oxidative stress exhibited by H_2O_2 on microbial communities may also increase (Wolf et al., 2018). However, understanding how changing conditions in light availability and CDOM concentrations will impact PH_2O_2 requires knowledge of how the major controls of PH_2O_2 each interact. In low CDOM waters, rates of photochemical processes increase with increasing CDOM (Cory et al., 2015). For example, PH_2O_2 may be limited by CDOM concentration (substrate) in low CDOM waters. Conversely, once CDOM concentrations are high enough to absorb all incoming light, PH_2O_2 remains constant with increasing CDOM. Under these conditions, photochemical processes are characterized as sunlight-limited (Cory et al., 2015). In addition to these limitations, the $\phi_{\text{H}_2\text{O}_2,\lambda}$ from CDOM may also be the dominant limiting factor (limitation by substrate composition). In all surface waters, each of these controls, along with water column depth, determine whether the water is substrate or light limited.

An understanding of the limitations of PH_2O_2 from $\phi_{\text{H}_2\text{O}_2,\lambda}$, CDOM concentrations, and sunlight availability will provide valuable insights to how surface waters and microbial communities may respond to changes in CDOM concentration (De Wit et al., 2021; Monteith et al., 2007; Williamson et al., 2015) and sunlight availability (Šmejkalová et al., 2016). Thus, the objectives of this study were: 1) quantify the magnitude and variability of the apparent quantum yield of H_2O_2 from CDOM ($\phi_{\text{H}_2\text{O}_2,\lambda}$) in arctic surface waters, and 2) predict the photochemical production of H_2O_2 (PH_2O_2) and quantify the influences of the $\phi_{\text{H}_2\text{O}_2,\lambda}$, CDOM concentrations, and sunlight on PH_2O_2 in arctic surface waters based on the expected ranges of these controls.

2. Methods

2.1 Sampling description & water analysis

Samples were collected from lakes and streams on the North Slope of Alaska in summer 2022 and 2023 (Figure 1). Lakes ranged from the Toolik Lake watershed (68.6318° N, 149.6060° W), the sentinel monitoring lake of the Arctic long-term ecological research station (LTER), to the coastal plain of the Alaskan Arctic. Stream water was collected from the Toolik Lake inlet, Sagavanirktok River, Colville River, and Oksrukuyik Creek. Water samples were collected in opaque, high-density polyethylene (HDPE) bottles. pH, specific conductance, and water temperature were measured in the field for all water samples using Orion or WTW pH and conductivity meters (Page et al., 2014; Trusiak et al., 2018). Water samples for H_2O_2 analysis were filtered with 0.2 μm Cytiva Whatman Polycap TC High-Capacity Capsules in the lab at Toolik Field Station immediately after collection. 0.2 μm -filtered water samples were stored in the dark at 4 °C until they were shipped in the dark on ice back to the lab at the University of Michigan. Once arriving at the lab at the University of Michigan, 0.2 μm -filtered water samples were stored in the dark at 4 °C until analysis of $\phi_{\text{H}_2\text{O}_2,\lambda}$.

Water that was analyzed for other chemistry parameters was filtered using Whatman glass fiber GF/F (nominal pore size 0.7 μm). GF/F filtered water samples were analyzed for dissolved organic carbon (DOC), CDOM, and total dissolved iron concentrations following previous work (Cory et al., 2014; Kling et al., 2000; Page et al., 2014). Analytical error for each measurement was reported based on averages of standard errors of field duplicate measurements in Toolik Lake, Toolik Inlet, and Oksrukuyik Creek from a summer 2023 Arctic LTER dataset (Table 1). DOC concentrations were measured on a Shimadzu TOC analyzer (Kling et al., 2000). CDOM absorption coefficients and optical proxies for composition of CDOM were measured on a Horiba Scientific Aqualog Spectrofluorometer (Cory et al., 2010) using 1 cm pathlength quartz cuvettes. Arctic surface waters are characterized by high concentrations of dissolved organic matter (DOM; Cory et al., 2007; Gareis et al., 2010). Given that DOM in forested streams and in arctic freshwaters is $\sim 80\%$ CDOM (Cory et al., 2014), CDOM is used to represent DOM in this study. Napierian CDOM absorption coefficients (a_{CDOM} , m^{-1}) were calculated by dividing decadic absorption coefficients obtained from analysis by cuvette pathlength (1 cm) and multiplying by 2.303 (Cory et al., 2007). CDOM spectral slope ratios (S_{R}), an optical proxy for molecular weight of DOM were calculated using the absorbance spectra measured in each water sample (Helms et al., 2008). Specific UV absorbance at 254 nm (SUVA_{254} , $\text{L} (\text{mg C})^{-1} \text{m}^{-1}$), a proxy for aromatic content in DOM, was calculated by dividing the decadic absorbance coefficient at 254 nm by the cuvette pathlength (1 cm) and DOC concentration (mg L^{-1}) in each water sample (Weishaar et al., 2003). Optical proxies for fluorescent dissolved organic matter (FDOM) were measured using an excitation emission matrix (EEM) on a Horiba Scientific Aqualog Spectrofluorometer with a 1 cm quartz pathlength cuvette (Cory et al., 2010). Using the measured EEM spectra, optical fluorescent dissolved organic matter (FDOM) composition proxies for the dominant fluorescence peaks A and T were quantified (Cory et al., 2010). Ratios of peak T to peak A were quantified as a proxy of the abundance of amino-acid like FDOM (Cory et al., 2010). Fluorescence index (FI), a proxy for the contributions of allochthonous versus autochthonous-derived DOM in FDOM was calculated in each water sample (Cory, et al., 2010; McKnight et al., 2001). Total dissolved iron concentrations were measured by inductively coupled plasma optical emission spectrometry (ICP-OES, Page et al., 2014).

H_2O_2 was measured in 0.2 μm -filtered water samples using an acridinium ester flow-injection chemiluminescence based method (FeLume; King et al., 2007). However, due to interference of dissolved iron with detection of H_2O_2 (Cooper et al., 2000; King et al., 2007), high iron water samples were excluded from this study ($> 5 \mu\text{M}$ total dissolved Fe).

2.2 H_2O_2 apparent quantum yield

The apparent quantum yield spectrum for H_2O_2 production from CDOM was quantified in 0.2 μm -filtered water samples ranging from three to seven months after being stored in the dark at 4 $^{\circ}\text{C}$. Water samples were brought to room temperature the day of light-exposure experiments. Prior to light exposure, an H_2O_2 standard calibration curve using 0.2 μm -filtered sample water was run using the FeLume method (King et al., 2007). H_2O_2 standards in sample water ranged from 0-1600 nM spikes of H_2O_2 . Subsets of each water sample were prepared for the light-exposure treatment in triplicates by placing water into gas-tight, flat-bottomed 12-mL quartz vials. A fourth vial was prepared for CDOM/FDOM analysis. Each of the four quartz vials were

exposed to light at five different wavelengths from the ultraviolet to visible light spectrum, using custom-built, high powered (100 mW), narrow-banded (± 10 nm) light emitting diodes (LEDs) at each wavelength (275, 305, 365, 385, & 405 nm, respectively), alongside dark controls (Bowen et al., 2020; Ward et al., 2021). Both dark controls and light exposed samples were kept at room temperature during the experiment using fans and heat sinks on LED chambers. LED irradiances were tuned such that the CDOM in each wavelength treatment absorbed equal amounts of light. Light exposure experiments were all conducted with the same amount of light absorbed at all wavelengths ($0.025 \text{ mol photons m}^{-2}$). This photon dose was calculated using a previously reported apparent quantum yield for H_2O_2 ($\phi_{\text{H}_2\text{O}_2,\lambda}$) from CDOM (Pandey et al., 2022) that results in the minimum detectable amount of H_2O_2 at 405 nm (~ 50 nM production of H_2O_2). The amount of light absorbed by CDOM ($\text{mol photons m}^{-2} \text{ nm}^{-1}$) in each experimental sample was quantified using absorbance coefficients measured immediately prior to light exposure and the LED photon flux spectrum as in previous work (Bowen et al., 2020; Cory et al., 2014; Ward et al., 2021). The photon flux spectrum from each wavelength LED chamber was quantified using radiometry as in previous work (Bowen et al., 2020).

H_2O_2 was measured in triplicate light-exposed samples immediately after completion of light exposure to minimize effects of decay, using the FeLume method (King et al., 2007). Each triplicate vial was measured using a set of three flow injections for a total of nine injections per wavelength treatment. Temperature was measured in each sample before analysis of H_2O_2 . In each sample, the amount of H_2O_2 produced was calculated from the amount of H_2O_2 measured minus the amount of H_2O_2 in each dark control. The fourth light-exposed sample was stored in the dark at room temperature after light-exposure and run on a Horiba Aqualog Spectrophotometer for fluorescence and absorbance for each wavelength treatment. In cases where the dark control experimental replicates were undetectable by the instrument, the concentration of H_2O_2 was assumed to be zero. Despite selecting waters for this study to minimize effects of iron interference, rapid decay in the chemiluminescent peak area was observed in sample replicates with concentrations of dissolved iron greater than $2 \mu\text{M}$. H_2O_2 is well understood to decay rapidly in the presence of dissolved iron via Photo-Fenton chemistry (Haber et al., 1934.; J H Festos, 1894.; Stumm & Lee 1961.; Vermilyea & Voelker, 2009; Zepp et al., 1992). Dissolved iron is known to cause interference with measurements of H_2O_2 using the FeLume method (Cooper et al., 2000; King et al., 2007). Decay as fast as 300 nM min^{-1} was observed in some samples at 275 nm and 305 nm wavelengths. In cases where rapid decay of peak area was observed, only the first replicate of each flow injection was used in quantifying the $\phi_{\text{H}_2\text{O}_2,\lambda}$.

Following light exposure, apparent quantum yield spectra were calculated for each experimental sample using the amount of H_2O_2 produced photochemically from CDOM (Equation 1, PH_2O_2 , light replicates minus dark controls at each wavelength, respectively), the duration of light exposure, LED irradiance ($E_{0,\lambda}$, Equation 2) and the amount of light absorbed by CDOM in each sample (Q_a , Equation 2).

$$\text{PH}_2\text{O}_2 = \int_{\lambda_{\min}}^{\lambda_{\max}} \phi_{\lambda} Q_a \quad \text{Equation 1}$$

$$Q_a = \int_{\lambda_{\min}}^{\lambda_{\max}} (1 - e^{-K_d \lambda z}) E_{0,\lambda} \quad \text{Equation 2}$$

The volume of each quartz tube (0.011 L) and concentration of H₂O₂ produced were used to determine the amount of mol H₂O₂ produced during light exposure. The surface area of each quartz vial (1.13 x 10⁻⁴ m²) was used to determine the amount of light absorbed by CDOM in each experiment. For each light exposure, CDOM was assumed to be the only light absorbing component in each water sample. The ϕ_{λ} is the only unknown in Equation 1 after light exposure, thus rearranging Equation 1 to solve for ϕ_{λ} produces an apparent quantum yield spectrum for H₂O₂ from CDOM. λ_{\min} and λ_{\max} in Equation 1 each represent the wavelength the $\phi_{\text{H}_2\text{O}_2,\lambda}$ was quantified at. Thus, a five-point $\phi_{\text{H}_2\text{O}_2,\lambda}$ spectrum was generated at wavelengths 275, 305, 365, 385, and 405 nm, respectively. The wavelength dependence of the $\phi_{\text{H}_2\text{O}_2,\lambda}$ was fit to an exponential decay model in the form of:

$$\phi_{\text{H}_2\text{O}_2,\lambda} = ce^{-d\lambda} \quad \text{Equation 3}$$

where parameters c (mol H₂O₂ mol photon⁻¹) and d (nm⁻¹) are positive constants. Matlab curve fitting application was used to obtain the exponential fit of the $\phi_{\text{H}_2\text{O}_2,\lambda}$ with 95% confidence intervals reported. 3 values of [H₂O₂] produced at each wavelength were used to obtain this exponential fit function.

2.3 Photochemical production rates of H₂O₂

Photochemical production rates of H₂O₂ in the water column (PH₂O₂, mmol H₂O₂ m⁻² day⁻¹, [Equation 4](#)) were calculated for all waters in this study using the $\phi_{\text{H}_2\text{O}_2,\lambda}$ (mmol H₂O₂ mol photons⁻¹) and the rate of light absorption by CDOM (Q_a , mol photons m⁻² day⁻¹ nm⁻¹, [Equation 2](#)).

$$\text{PH}_2\text{O}_2 = \int_{\lambda_{\min}}^{\lambda_{\max}} \phi_{\lambda} Q_a \frac{a_{\text{CDOM}}}{a_{\text{TOT}}} \quad \text{Equation 4}$$

λ_{\min} and λ_{\max} represent 280 nm to 600 nm, respectively, encompassing the range of UV to visible light in the solar spectrum. The fraction of light absorption by CDOM in the water column was represented by $a_{\text{CDOM}}/a_{\text{TOT}}$ in [Equation 4](#) (with a_{TOT} representing the total absorbance from the water column). For this study, $a_{\text{CDOM}}/a_{\text{TOT}}$ was assumed to be 1. That is, CDOM was assumed to be the only light absorbing component of arctic surface waters (Cory et al., 2014; Cory et al., 2015).

PH₂O₂ was calculated two ways for this study: maximum PH₂O₂ for each water in this study at peak solar zenith angle, and daily PH₂O₂ in Toolik Lake every summer (May-October) throughout the period 2012-2023. The former calculation of PH₂O₂ used CDOM absorption spectra measured for each sample in this study ([Table 1](#)) to calculate the rate of light absorption by CDOM (Q_a , [Equation 2](#)). Daily PH₂O₂ in Toolik Lake was calculated using average CDOM absorbance spectra for each month of each summer (May-October) from the period 2012-2023. Average water column depth (z , [Equation 4](#)) for each water in this study was used for calculations of PH₂O₂. The $\phi_{\text{H}_2\text{O}_2,\lambda}$ measured for each water in this study was used to calculate PH₂O₂. Daily photon fluxes reaching Toolik Lake were collected every day in the summer (15-May through 1-October) from 2012-2023 by the Arctic LTER and Toolik Field Station. Photon fluxes ($E_{0,\lambda}$, [Equation 2](#)) for peak solar zenith angle (i.e. summer solstice) were used to calculate maximum PH₂O₂ for all waters in this study. Photon fluxes for each day they were recorded were

used to calculate daily PH_2O_2 in Toolik Lake. For each day that photon fluxes were recorded at Toolik Field Station, a modeled irradiance for clear-sky conditions was produced from SMARTS version 295 PC. Cloudiness for each day that photon fluxes were measured at Toolik Field Station was calculated using the ratio of measured irradiance to modeled clear-sky irradiance from SMARTS.

To investigate the sensitivity of PH_2O_2 to the amount of sunlight absorbed, CDOM concentrations, or $\phi\text{H}_2\text{O}_{2,\lambda}$, each term was varied independently while the others were held constant (Equation 4). When varying each term, the maximum, minimum, and average values were used. For example, maximum photon flux is observed when solar zenith angle is at its peak, and minimum photon flux is observed at the end of the summer when solar zenith angle is much lower. Maximum and minimum values were calculated for the $\phi\text{H}_2\text{O}_{2,\lambda}$ for each water in this study using ± 1 standard error. Variation in the CDOM absorption spectra used the maximum, minimum, and average $a\text{CDOM}$ (a_{305} , m^{-1}) values from years 2012-2023 for each water in this study from an Arctic LTER dataset. Sensitivity tests were performed in two groupings: the Toolik Lake watershed, and the coastal plain. Some experimental sites were excluded from the sensitivity groupings (LTER 345, Fog 01, Sagavanirktok River, Oksrukuyik Creek) due to spatial variations from the rest of the sites.

Another sensitivity test on PH_2O_2 was performed only for Toolik Lake to observe the non-linear response of PH_2O_2 to increasing CDOM (Equation 4). In this test, photon fluxes for peak solar zenith angle and the measured $\phi\text{H}_2\text{O}_{2,\lambda}$ for Toolik Lake were used while varying concentration of CDOM. A range of typical CDOM concentrations for Toolik Lake were used in this sensitivity test. Additionally, average CDOM concentrations of Toolik Lake were scaled up and down by factors of 1.5, 2, and 3, respectively when calculating PH_2O_2 to simulate projected increases or decreases in CDOM concentration.

3. Results

3.1 Water and DOM chemistry

The pH for all waters sampled in this study ranged from 6.6 - 8.5 (Table 1). Specific conductance ranged from 22.9-345 $\mu\text{S}/\text{cm}$ as expected based on landscape age (Keller et al., 2007; Page et al., 2013; Trusiak et al., 2018; Walker & Everett, 1991). Water temperature varied by the date of sample collection over the summer, with the highest temperatures recorded in waters that were sampled later in the summer season. Dissolved iron (Fe) for all waters in this study were within the typical range of low-iron arctic freshwaters, ranging from 0.11 - 6.47 $\mu\text{M} \pm 0.002$ (Bowen et al., 2020; Page et al., 2013, 2014; Trusiak et al., 2018, 2019).

The composition of CDOM and chemistry of waters sampled in this study were similar to prior work on waters in the same location as this study (Table 1; Cory et al., 2014; Cory et al., 2007). Dissolved organic carbon concentrations (DOC) ranged from 122 - 957 ± 3.15 μM . CDOM concentrations (a_{305} , m^{-1}) ranged from 5.90 - 39.9 ± 0.13 m^{-1} . DOC and CDOM concentrations were in the expected range for arctic surface waters (Cory et al., 2014; Cory et al., 2007; Kling et al., 2000).

Optical proxies for DOM composition were also in the expected range (Table 1; Cory et al., 2014; Cory et al., 2007). Spectral slope ratio (S_R), a unitless term that is an optical proxy for the molecular weight of the DOM in water (Helms et al., 2008) ranged from 0.82 - 1.89 ± 0.02 . $SUVA_{254}$ values ($L (mg C)^{-1} m^{-1}$), a proxy for the aromaticity of the DOM in water (Weishaar et al., 2003) ranged from 1.78 - $3.60 \pm 0.03 L (mg C)^{-1} m^{-1}$. DOM for all waters in this study had similar fluorescence indexes (FI), a proxy for contributions of allochthonous versus autochthonous-derived DOM in FDOM (Cory et al., 2010; McKnight et al., 2001) ranging from 1.41- 1.55 ± 0.01 . Peak T/A ratios, a proxy for the abundance of amino-acid like FDOM (Cory et al., 2010), ranged from 0.12 - 0.33 ± 0.02 .

3.2 Photon fluxes

The daily photon flux varied with solar zenith angle (e.g., date and latitude), and cloudiness. Daily photon fluxes peaked when the zenith angle was highest (i.e., at the summer solstice) and then decreased throughout the summer through fall as the zenith angle decreased (Figure S1). Daily photon fluxes across the whole summer varied depending on cloudiness. The variability in light availability due to cloudiness is reflected by the ratio of measured photon fluxes to modeled clear sky conditions (Figure S2). No summer showed a significantly higher or lower than average daily photon flux over the period 2012-2023 (Figure S3).

3.3 H₂O₂ apparent quantum yield spectra

The H₂O₂ apparent quantum yield spectra ($\phi_{H_2O_2,\lambda}$) decreased exponentially with increasing wavelength (Figure 2). The $\phi_{H_2O_2,305}$ ranged from 0.84 ± 0.02 mmol H₂O₂ mol photons⁻¹ to 3.28 ± 0.04 mmol H₂O₂ mol photons⁻¹ (Table 2). The $\phi_{H_2O_2,405}$ ranged from 0.07 ± 0.001 to 0.58 ± 0.01 mmol H₂O₂ mol photons⁻¹ (Table 2). The slope of the exponential fit functions of $\phi_{H_2O_2,\lambda}$ spectra were calculated using Matlab with 95% confidence intervals, ranging from -0.017 to -0.026 (± 0.003) mmol H₂O₂ mol photons⁻¹ nm⁻¹.

The $\phi_{H_2O_2,365}$ was strongly, positively correlated with $SUVA_{254}$ ($p < 0.005$) and the $\phi_{H_2O_2,305}$ was strongly, negatively correlated with spectral slope ratio ($p < 0.05$) (Figure 3a, b). Other optical proxies such as fluorescence index and peak T/A ratios were not significantly correlated with the $\phi_{H_2O_2,\lambda}$. The $\phi_{H_2O_2,275}$ was strongly, positively correlated with dissolved iron for all waters measured in this study (Figure 4, $p < 0.05$).

3.4 Photochemical H₂O₂ production rates

The PH_2O_2 at the peak solar zenith angle ranged from 1.47 mmol H₂O₂ m⁻² day⁻¹ to 7.74 mmol H₂O₂ m⁻² day⁻¹ across all waters (Figure S4). Daily PH_2O_2 in Toolik Lake was highest at the peak solar zenith angle and decreased throughout the summer during the period 2012-2023. Daily PH_2O_2 in Toolik Lake ranged from 4.16 mmol H₂O₂ m⁻² day⁻¹ at the peak solar zenith angle to 0.16 mmol H₂O₂ m⁻² day⁻¹ at the end of the summer (Figure S5a,b).

A sensitivity analysis comparing the effects of light availability (i.e. photon flux), CDOM concentration and the $\phi_{H_2O_2,\lambda}$ showed that the PH_2O_2 was most strongly limited by sunlight availability (Figure 5). That is, PH_2O_2 varied approximately three-fold from the minimum to

maximum photon fluxes. Photon fluxes varied by approximately ten-fold from their minimum to maximum. PH_2O_2 increased linearly with increasing photon fluxes (Figure S6). PH_2O_2 was also limited by CDOM (substrate) concentration and composition. For example, PH_2O_2 varied by approximately $\frac{1}{3}$ fold from the minimum to maximum CDOM concentrations. CDOM concentrations in all waters varied by approximately ten-fold from their minimum to maximum. Likewise, PH_2O_2 varied by approximately $\frac{1}{3}$ -fold from the minimum to maximum $\phi\text{H}_2\text{O}_{2,\lambda}$. The $\phi\text{H}_2\text{O}_{2,\lambda}$ in all waters varied by approximately 1.5-fold from their minimum to maximum.

However, limitations of PH_2O_2 can vary over the summer season in any water. For example, in Toolik Lake, PH_2O_2 increases non-linearly with increasing CDOM concentration (as expected from Equation 4; Figure 6). When CDOM concentrations are on the low end of the range observed in Toolik Lake (Figure 6), PH_2O_2 increases linearly with increasing CDOM. At the high end of CDOM concentrations in Toolik Lake, increasing CDOM concentrations $> 15 \text{ m}^{-1}$ at 305 nm has no impact on PH_2O_2 . Low concentrations of CDOM in Toolik Lake are expected late in the summer, where light availability is also at its lowest. High concentrations of CDOM in Toolik Lake occur early in the ice-off season, when solar zenith angle is at its peak. Thus, considering the temporal patterns in CDOM and light availability in the limitation on PH_2O_2 , PH_2O_2 will be light limited in early season just after ice off, and substrate limited in late summer season.

4. Discussion

4.1 The $\phi\text{H}_2\text{O}_{2,\lambda}$ in arctic surface waters are higher than reported in other freshwaters and seawater

The $\phi\text{H}_2\text{O}_{2,\lambda}$ measured in arctic surface waters were all of higher magnitude than reported for seawater $\phi\text{H}_2\text{O}_{2,\lambda}$ (Figure 2; Andrews et al., 2000; Kieber et al., 2014; Powers & Miller, 2014). The $\phi\text{H}_2\text{O}_{2,\lambda}$ measured in arctic surface waters were also higher magnitude than other $\phi\text{H}_2\text{O}_{2,\lambda}$ reported for freshwaters (Cooper et al., 1988; O'Sullivan et al., 2005; Pandey et al., 2022; Scully et al., 1996). The $\phi\text{H}_2\text{O}_{2,\lambda}$ for the Maumee River reported in Pandey et. al 2022 is the most similar $\phi\text{H}_2\text{O}_{2,\lambda}$ in magnitude and shape to $\phi\text{H}_2\text{O}_{2,\lambda}$ measured in arctic surface waters. However, the $\phi\text{H}_2\text{O}_{2,275}$ for the Maumee River was approximately $2 \text{ mmol H}_2\text{O}_2 \text{ mol photons}^{-1}$, while the $\phi\text{H}_2\text{O}_{2,275}$ for some waters in this study (Toolik Inlet, I8, Oks Creek, LHS 2-01) were more than double this $\phi\text{H}_2\text{O}_{2,275}$ in the Maumee River. On average, the $\phi\text{H}_2\text{O}_{2,305}$ for all waters measured in this study is higher than all reported values at $\sim 305 \text{ nm}$ from the literature (Andrews et al., 2000; Kieber et al., 2014; O'Sullivan et al., 2005; Pandey et al., 2022; Powers & Miller, 2014). The exponential decay of $\phi\text{H}_2\text{O}_{2,\lambda}$ as a function of wavelength observed in all samples is expected based on previous work that investigated the wavelength dependence of $\phi\text{H}_2\text{O}_{2,\lambda}$ (Andrews et al., 2000; Pandey et al., 2022; Wu et al., 2021).

4.2 The $\phi\text{H}_2\text{O}_{2,\lambda}$ confirm the importance of terrestrially derived CDOM on the magnitude of $\phi\text{H}_2\text{O}_{2,\lambda}$

The dominant form of CDOM in arctic freshwaters the late spring/early summer is terrestrially derived CDOM exported from land via snowmelt into streams and lakes (Michaelson et al.,

1998). Previous work in freshwaters at lower latitudes concluded that the fraction of CDOM (and thus terrestrially-derived CDOM) is an important control on the magnitude of the H_2O_2 apparent quantum yield spectra from CDOM ($\phi_{\text{H}_2\text{O}_2,\lambda}$; O'Sullivan et al., 2005; Pandey et al., 2022; Powers & Miller, 2014). Multiple lines of evidence found in the $\phi_{\text{H}_2\text{O}_2,\lambda}$ for arctic surface waters support these findings.

The primary line of evidence to support that terrestrially-derived CDOM controls the magnitude of $\phi_{\text{H}_2\text{O}_2,\lambda}$ is the significant relationships between $\phi_{\text{H}_2\text{O}_2,\lambda}$ and optical proxies for CDOM composition (Figure 3a, b). Both the significant, negative relationship between $\phi_{\text{H}_2\text{O}_2,305}$ and spectral slope ratio (Figure 3a) and the significant, positive relationship between CDOM aromaticity and $\phi_{\text{H}_2\text{O}_2,365}$ (Figure 3b) in the waters measured in this study support the finding that terrestrially-derived CDOM controls the magnitude of the $\phi_{\text{H}_2\text{O}_2,\lambda}$. High molecular weight, aromatic CDOM is typically associated with CDOM of terrestrial origin (Helms et al., 2008; Weishaar et al., 2003). Pandey et. al 2022 observed a similarly significant, positive relationship between SUVA_{254} and $\phi_{\text{H}_2\text{O}_2,350}$ in all samples from their study. Inclusion of SUVA_{254} and $\phi_{\text{H}_2\text{O}_2,350}$ values from Pandey et. al 2022 displayed strong agreement with SUVA_{254} and $\phi_{\text{H}_2\text{O}_2,365}$ for waters in this study (Figure 3b). The highest reported SUVA_{254} value in Pandey et. al 2022 was $2.97 \pm 0.18 \text{ L mg C}^{-1} \text{ m}^{-1}$ for the Maumee River. Nearly half of all of the waters in this study had SUVA_{254} values greater than $3 \text{ L mg C}^{-1} \text{ m}^{-1}$ (Table 1), and each of these sites had higher magnitude $\phi_{\text{H}_2\text{O}_2,\lambda}$ than the Maumee River. Each of the highest magnitude $\phi_{\text{H}_2\text{O}_2,\lambda}$ measured for waters in this study had the highest SUVA_{254} values. This finding can explain why some of the waters measured in this study had $\phi_{\text{H}_2\text{O}_2,\lambda}$ that were much higher than the $\phi_{\text{H}_2\text{O}_2,\lambda}$ in the Maumee River, assuming that the $\phi_{\text{H}_2\text{O}_2,\lambda}$ is strongly dependent on SUVA_{254} .

Timing of sample collection for this study also provides compelling evidence that the magnitude of $\phi_{\text{H}_2\text{O}_2,\lambda}$ is controlled by organic matter composition. Except for water samples collected from lakes on the coastal plain, all waters measured in this study were collected near or before the summer solstice when CDOM in lakes is strongly terrestrially derived (Cory et al., 2007). High magnitude $\phi_{\text{H}_2\text{O}_2,\lambda}$ measured in arctic surface waters during this time-frame is in agreement with the composition of CDOM being a primary control on the magnitude of $\phi_{\text{H}_2\text{O}_2,\lambda}$. As the proportion of terrestrially derived CDOM decreases throughout the summer (Michaelson et al., 1998), the $\phi_{\text{H}_2\text{O}_2,\lambda}$ should also decrease. This expectation is consistent with Pandey et. al 2022 finding that the $\phi_{\text{H}_2\text{O}_2,\lambda}$ decreased in magnitude in Lake Erie significantly from June to October.

Previous work suggested that the magnitude of $\phi_{\text{H}_2\text{O}_2,\lambda}$ depended on the proportion of terrestrially derived CDOM (O'Sullivan et al., 2005; Pandey et al., 2022; Powers & Miller, 2014), but found no significant correlation between any proxy for CDOM composition and the $\phi_{\text{H}_2\text{O}_2,\lambda}$. O'Sullivan et. al 2005 compared the $\phi_{\text{H}_2\text{O}_2,\lambda}$ between river water and coastal water, and suggested the higher magnitude $\phi_{\text{H}_2\text{O}_2,\lambda}$ in river water was due to the proportion of terrestrially derived CDOM. Powers and Miller 2014 also suggested that higher magnitude $\phi_{\text{H}_2\text{O}_2,\lambda}$ in freshwaters may be due to the proportion of terrestrially-derived CDOM. Pandey et. al 2022 found a statistically significant relationship between SUVA_{254} and $\phi_{\text{H}_2\text{O}_2,350}$, consistent with the findings in this study (Figure 3b, $p < 0.0005$ vs. $p < 0.05$).

One potential reason for the lack of relationships between CDOM composition and the $\phi_{\text{H}_2\text{O}_2,\lambda}$ in prior work (Andrews et al., 2000; Kieber et al., 2014; O'Sullivan et al., 2005; Pandey et al.,

2022; Powers & Miller, 2014), is that the $\phi_{\text{H}_2\text{O}_2,\lambda}$ were measured using differing amounts of light absorbed between waters and at each wavelength. However, Andrews et. al 2000 demonstrated that $\phi_{\text{H}_2\text{O}_2,\lambda}$ are dose dependent (i.e. the $\phi_{\text{H}_2\text{O}_2,\lambda}$ decreases at each wavelength with light exposure time). Thus, a disadvantage of measuring $\phi_{\text{H}_2\text{O}_2,\lambda}$ with different amount of light absorbed that the $\phi_{\text{H}_2\text{O}_2,\lambda}$ may be more dependent on the amount of light absorbed by CDOM than on the composition of CDOM. For this study, all $\phi_{\text{H}_2\text{O}_2,\lambda}$ were measured with equal lights absorbed by CDOM at all wavelengths (see methods). This approach removes the effect of light dose (and light absorbed) on the AQY, thus allowing an assessment of the dependence of $\phi_{\text{H}_2\text{O}_2,\lambda}$ on CDOM composition.

4.3 Dissolved iron concentrations may control the magnitude of $\phi_{\text{H}_2\text{O}_2,\lambda}$

It is well understood that H_2O_2 and dissolved iron (Fe) are closely coupled in surface waters via Fenton Chemistry (Haber et al., 1934.; J H Festos, 1894.; Stumm & Lee 1961.; Vermilyea & Voelker, 2009; Zepp et al., 1992). For example, in sunlit waters, H_2O_2 can act as a strong oxidant of Fe(II) and produce Fe(III) and hydroxyl radical ($\cdot\text{OH}$). Further, evidence suggests strong coupling of dissolved iron and formation of $\cdot\text{OH}$ in arctic surface waters (Page et al., 2014). Thus, it is reasonable to expect that photo-Fenton reaction occurs readily in arctic surface waters (Hammerschmidt & Fitzgerald, 2010; Page et al., 2014). There is no known minimum iron concentration at which is required for Fenton chemistry to occur, but the higher the dissolved iron concentration, the more important the Fenton reaction is expected to be (Vermilyea et al. 2009). In arctic freshwaters where total dissolved iron concentrations are much higher than most freshwaters ($> 5 \mu\text{M}$; Bowen et al., 2020; Page et al., 2013, 2014; Trusiak et al., 2018, 2019), Fenton chemistry should influence H_2O_2 production. If Fenton chemistry is a dominant process in high iron waters with H_2O_2 , then Fenton chemistry likely influences the $\phi_{\text{H}_2\text{O}_2,\lambda}$ in arctic surface waters as well. In this study, total dissolved iron concentrations were significantly, positively correlated with $\phi_{\text{H}_2\text{O}_2,275}$ ($p < 0.05$, [Figure 4](#)). This result is consistent with a relationship between the formation of $\cdot\text{OH}$ and dissolved iron in arctic surface waters over a wider range of iron concentrations than in this study (Page et al., 2014). Waters in this study ranged from 0.1 - 6.5 (± 0.002) μM total dissolved iron ([Table 1](#)), which is on the low end reported in arctic freshwaters (Bowen et al., 2020; Page et al., 2013, 2014; Trusiak et al., 2018, 2019). Thus, the dependence of $\phi_{\text{H}_2\text{O}_2,\lambda}$ on dissolved iron in arctic surface waters may be underestimated due to the limitation of measuring H_2O_2 in high iron waters. The implication is that the $\phi_{\text{H}_2\text{O}_2,\lambda}$ and photochemical production rates of H_2O_2 reported in this study are a minimum, given that only low iron waters were sampled.

4.4 Photochemical production rates of H_2O_2 in arctic surface waters are high compared to lower latitude freshwaters

When photochemical production of H_2O_2 (PH_2O_2) was calculated for arctic surface waters using photon fluxes at peak solar zenith angle, the absorption spectra from CDOM (a_{CDOM}) for date of collection of the sample, and $\phi_{\text{H}_2\text{O}_2,\lambda}$ measured experimentally ([Equation 4](#)), PH_2O_2 was higher than freshwaters reported in the literature, on average (Cory et al., 2016; Jerome & Bukata, 1998; Pandey et al., 2022; [Figure S4](#)). On average, PH_2O_2 for arctic surface waters was $3.67 \pm 0.39 \text{ mmol H}_2\text{O}_2 \text{ m}^{-2} \text{ day}^{-1}$ ([Figure S4](#), approximately 1.5-fold higher than the $2.6 \pm 0.2 \text{ mmol H}_2\text{O}_2 \text{ m}^{-2} \text{ day}^{-1}$ reported for early season Lake Erie in Pandey et. al 2022. PH_2O_2 for this

study was predicted to be as high as $7.74 \text{ mmol H}_2\text{O}_2 \text{ m}^{-2} \text{ day}^{-1}$ (Figure S4), which is nearly three-fold higher than the value of PH_2O_2 reported in Pandey et. al 2022. There are a few factors that contribute to the significantly higher PH_2O_2 expected in arctic surface waters. First, the magnitude of $\phi_{\text{H}_2\text{O}_2,\lambda}$ measured in arctic surface waters was significantly higher than any $\phi_{\text{H}_2\text{O}_2,\lambda}$ measured for Lake Erie at all wavelengths (Pandey et al., 2022). PH_2O_2 increases linearly with increasing $\phi_{\text{H}_2\text{O}_2,\lambda}$ (Equation 4). Secondly, many of the slopes of $\phi_{\text{H}_2\text{O}_2,\lambda}$ exponential best fit functions were significantly shallower for waters in this study than lower latitude freshwaters (Pandey et al., 2022). A shallower slope for $\phi_{\text{H}_2\text{O}_2,\lambda}$ leads to higher $\phi_{\text{H}_2\text{O}_2,\lambda}$ at higher wavelengths (Figure 2). Because greater amounts of visible light (400-700 nm) reach the water than UV light, the magnitude of PH_2O_2 if $\phi_{\text{H}_2\text{O}_2,\lambda}$ is higher at visible wavelengths when the slope for $\phi_{\text{H}_2\text{O}_2,\lambda}$ is relatively shallow in the visible range compared to a slope that decreases more strongly with wavelength from the UV to the visible range (Equation 4). The third reason for higher expected PH_2O_2 in arctic surface waters compared to lower latitude freshwaters is due to differences in CDOM concentrations in arctic vs. other freshwaters. PH_2O_2 increases non-linearly with increasing CDOM concentrations (Equation 4), and arctic surface waters have significantly higher CDOM concentrations than Lake Erie (Table 1, Cory et al., 2016; Pandey et al., 2022). Higher concentrations of CDOM lead to greater amounts of light absorbed according to Equation 4, thus resulting in higher PH_2O_2 . The final reason for higher expected PH_2O_2 in arctic surface waters is the assumption that CDOM is the only light absorbing component in the water column. In arctic surface waters characterized by low biomass and oligotrophy (Kling et al., 2000), CDOM is the main light-absorbing constituent and thus $a_{\text{CDOM}}/a_{\text{TOT}}$ (Equation 4) is equal to 1 (Cory et al., 2014; Cory et al., 2015). In waters like Lake Erie, the absorption of light by biomass from algae blooms results in particles other than CDOM that absorb and scatter incoming sunlight, decreasing the fraction of light absorbed by CDOM (Cory et al., 2016; Pandey et al., 2022). As the fraction of light absorbed by CDOM decreases, so does PH_2O_2 (Equation 4).

4.5 Controls on photochemical H_2O_2 production

Sensitivity tests performed on the controls of PH_2O_2 in arctic surface waters showed that PH_2O_2 is most limited by light availability and can also be co-limited by substrate (Figure 5). The strong, linear dependence of PH_2O_2 on light availability suggests that variations in light availability should change PH_2O_2 similarly. This linear dependence coupled with the 10-fold range of photon fluxes from their minimum to maximum (Figure S1) result in strong light limitation of PH_2O_2 . Both cloud cover and seasonal variation in solar zenith angle can cause photon fluxes reaching the surface to vary on a daily and monthly timescale (Figure S1). Because PH_2O_2 is strongly light-limited, the production of H_2O_2 varies by a factor of 4 over the summer season. For example, maximum daily PH_2O_2 (Figure S5b, $4.16 \text{ mmol H}_2\text{O}_2 \text{ m}^{-2} \text{ day}^{-1}$) was calculated in Toolik Lake near the peak solar zenith angle in the early summer season, while minimum daily PH_2O_2 (Figure S5b, $0.16 \text{ mmol H}_2\text{O}_2 \text{ m}^{-2} \text{ day}^{-1}$) was calculated at the end of the summer. Daily PH_2O_2 in Toolik Lake was also strongly, positively correlated with daily total photon flux (Figure S6).

Ice-off date in arctic surface waters is occurring earlier each year (Šmejkalová et al., 2016), thus increasing the number of days that surface waters are exposed to light. Because ice-off typically occurs near peak solar zenith angle, the increased exposure of surface waters to sunlight due to

earlier ice-off will increase exposure of waters to incoming sunlight. However, cloudiness is also expected to increase on the arctic landscape (Kay & Gettelman, 2009), which would decrease exposure of surface waters to sunlight and decrease PH_2O_2 . Ice-cover on lakes allows snow to build up on the surface of the ice, which prevents penetration of UV and visible light into the water column. Moreover, cloudiness and cloud cover decrease the penetration of UV and visible light, but not as completely as ice covered by snow does.

Photon fluxes reaching the surface of arctic surface waters are considerably lower than photon fluxes at lower latitudes (Figure S7). A higher zenith angle at higher latitudes causes light availability to be lowered due to a longer atmospheric pathlength and thus greater scattering compared to lower latitude freshwaters. Thus, high PH_2O_2 in arctic surface waters must be influenced strongly by substrate composition and composition, even if most limited by light availability. This expectation is consistent with arctic surface waters characterized by high concentrations of CDOM and high proportions of terrestrially derived organic matter (Cory et al., 2014; Cory et al., 2007; Kling et al., 2000; Whalen & Cornwell, 1985). Seasonal shifts in CDOM concentrations and CDOM origin likely contribute to the expected decline in PH_2O_2 throughout the summer. Early summer snowmelt conditions coincide with high export of terrestrially derived CDOM from streams to lakes (Michaelson et al., 1998). Thus, we would expect the $\phi_{\text{H}_2\text{O}_2, \lambda}$ to be highest in the early season, when $a\text{CDOM}$ is known to be highest (Cory et al., 2007). PH_2O_2 should be highest when all three variables are also highest, as light availability peaks at similar times to both $a\text{CDOM}$ and the proportion of terrestrially derived CDOM. These expectations emphasize that despite being limited mostly by light, the concentration and composition of CDOM also influence the magnitude of PH_2O_2 .

The sensitivity of PH_2O_2 in Toolik Lake to CDOM concentration (a_{305} , m^{-1}) is non-linear (Figure 6, Equation 4). Thus, substrate limitation should occur in low CDOM waters. For example, CDOM concentrations lower than 15 m^{-1} at 305 nm in Toolik Lake result in substrate limitation of PH_2O_2 . Previous work suggested that the influence of H_2O_2 on oxidative stress will increase due to browning of boreal freshwaters (Wolf et al., 2017, 2018). Wolf et al. 2018 reported a wide range of modeled CDOM concentrations in the UV range (a_{305} , $5 - 80 \text{ m}^{-1}$) based off field measurements in the visible range ($a_{400-700}$). This work demonstrates that in high CDOM waters (eg. a_{305} 15 m^{-1} or higher), light availability is more important than substrate availability, thus the browning of freshwaters occurring throughout North American and European freshwaters (De Wit et al., 2021; Monteith et al., 2007; Williamson et al., 2015) may not affect oxidative stress as previously thought. For example, increasing average CDOM concentrations ($a_{305} \sim 15 - 17 \text{ m}^{-1}$) in Toolik Lake by a factor of 2 ($a_{305} \sim 30 \text{ m}^{-1}$) did not significantly change the magnitude of PH_2O_2 at the peak solar zenith angle (Figure 6). In waters more susceptible to substrate limitation of PH_2O_2 , the browning of freshwaters may significantly increase the effects of oxidative stress on microbial communities. One such example is a low CDOM lake with high residence time that receives small amounts of CDOM input throughout the ice-off season. In this substrate-limited lake, the magnitude of PH_2O_2 should increase in response to the expected increase of CDOM concentrations in freshwaters. However, because of the strength of light limitation on PH_2O_2 , substrate limited waters should also be limited by light availability. Conversely, light limited waters are not necessarily substrate-limited, as shown by the non-linear response of PH_2O_2 to increasing CDOM. Results from these sensitivity tests indicate that substrate vs. light limitation of PH_2O_2 is highly dependent on the type of water.

4.6 Estimated steady state concentrations of [H₂O₂] in Toolik Lake

Using average PH₂O₂ for Toolik Lake across all years, one can estimate steady-state concentrations of H₂O₂ in Toolik Lake. Previously reported biological production rates of H₂O₂ range from 1 - 6 mmol H₂O₂ m⁻² day⁻¹ in eutrophic waters (Cory et al., 2016; Marsico et al., 2015). Arctic waters characterized by low-productivity and oligotrophy are unlikely to support high biological production rates. Thus, we assume that for arctic surface waters, photochemical production of H₂O₂ by light absorption of CDOM is the only source of H₂O₂ in these waters. Conversely, because these waters are oligotrophic, it is reasonable to assume that biological decay of H₂O₂ is low, compared to more productive freshwaters. Previous work showed that biological decay of H₂O₂ increases with increasing cell counts, a measure of microbial biomass and activity (Cooper et al., 1994; Marsico et al., 2015), and decay rate constants are highest in eutrophic waters (> 1.0 hour⁻¹). For this study, a first order decay constant for an oligotrophic lake (k_{loss} , 0.14 hour⁻¹, Marsico et al., 2015), was used to calculate steady state concentrations of H₂O₂. On average, steady state concentrations of H₂O₂ in Toolik Lake are 500 nM. Steady state concentrations can reach as high as 1000 nM using the maximum predicted daily PH₂O₂ for Toolik Lake, and 50 nM using the minimum predicted daily PH₂O₂. These estimated concentrations are within the range measured in freshwater lakes (10 nM - 2 μ M, Cooper et al., 1988, 1989; Cory et al., 2016; Häkkinen et al., 2004; Scully et al., 1996).

The estimated concentrations of H₂O₂ in Toolik Lake are within the range expected to cause oxidative stress on aquatic microorganisms (Drábková et al., 2007; Latifi et al., 2009; Lesser, 2006). For example, previous work has shown that concentrations as low as 50 nM can exert oxidative stress on microbial communities (Leunert et al., 2014). Thus, the estimated concentrations of H₂O₂ in Toolik Lake may cause oxidative stress to microorganisms, and in turn, affect microbial community composition. Previous work in Toolik Lake found that bacterial communities vary strongly from the surface waters to bottom waters (Crump et al., 2012). The difference in bacterial communities was primarily attributed to surface water inoculation of taxa from the Toolik Lake inlet stream, but the results of this study suggest that oxidative stress from H₂O₂ could be a strong influence on Toolik Lake microbial community composition. Assuming photochemical production of H₂O₂ from CDOM is the only source of H₂O₂ in the lake, estimated concentrations of H₂O₂ should be highest in the surface of the lake, where light can penetrate. Thus, high concentrations of H₂O₂ in the surface water compared to bottom waters of Toolik Lake may contribute to differences in microbial community composition.

However, the estimated steady state concentration of H₂O₂ in Toolik Lake may be an underestimate because of second order decay of H₂O₂ via Photo-Fenton chemistry. Fenton chemistry is suggested to occur in high iron arctic surface waters (Hammerschmidt & Fitzgerald, 2010; Page et al., 2014). The second order rate constant for decay of H₂O₂ by the Fenton reactions depends both on Fe(II) and H₂O₂ concentrations. Total dissolved iron concentrations in Toolik Lake are low for arctic surface waters (<1 μ M, Page et al., 2013, 2014; Trusiak et al., 2018, 2019), thus the effect of Photo-Fenton chemistry on H₂O₂ in Toolik Lake is likely not as high as it can be in other higher iron waters.

5. Conclusions

The $\phi_{\text{H}_2\text{O}_{2,\lambda}}$ in arctic surface waters were of higher magnitude than other freshwaters and seawater, as expected. Results of this study confirm that the chemical composition of organic matter is a strong predictor of the $\phi_{\text{H}_2\text{O}_{2,\lambda}}$, and suggest that dissolved iron is an important control on the $\phi_{\text{H}_2\text{O}_{2,\lambda}}$. Aromatic, high molecular weight dissolved organic matter and dissolved iron were strongly, positively correlated with the $\phi_{\text{H}_2\text{O}_{2,\lambda}}$ from CDOM. These results provide a framework for predicting the magnitude of $\phi_{\text{H}_2\text{O}_{2,\lambda}}$ as a function of CDOM composition, in light of changing environmental conditions in the Arctic. For example, decreasing aromatic content of CDOM in arctic surface waters as the summer ice-off season progresses (Cory et al., 2014; Cory et al., 2007) should result in a decrease in $\phi_{\text{H}_2\text{O}_{2,\lambda}}$. Thus, we expect the $\phi_{\text{H}_2\text{O}_{2,\lambda}}$ to vary over the ice-free summer in arctic surface waters. As the arctic warms and thaw deepens in permafrost soils, CDOM from the previously frozen permafrost mineral soil layers will be flushed into arctic surface waters (Feng et al., 2013). Permafrost CDOM has a lower aromaticity than CDOM draining from active layer soils (Bowen et al., 2020; Cory et al., 2013; Ward & Cory, 2015, 2016). However, permafrost soils may also be high in iron, and thus export of this material laterally so surface waters may increase export of dissolved iron to surface waters (Bowen et al., 2020; Trusiak et al., 2019). The results in this study predict that the $\phi_{\text{H}_2\text{O}_{2,\lambda}}$ should decrease with decreasing CDOM aromaticity, but increase with increasing dissolved iron concentrations. Thus, the overall effect of shifting CDOM sources on $\phi_{\text{H}_2\text{O}_{2,\lambda}}$ as permafrost soils thaw may depend on the importance of CDOM aromaticity vs. dissolved iron concentrations for determining $\phi_{\text{H}_2\text{O}_{2,\lambda}}$. The influence of dissolved iron on the $\phi_{\text{H}_2\text{O}_{2,\lambda}}$ was not a primary focus of this study, but it is likely important given the close coupling of dissolved iron and $\cdot\text{OH}$ formation in arctic surface waters via Photo-Fenton chemistry (Page et al., 2014). We would expect $\phi_{\text{H}_2\text{O}_{2,\lambda}}$ to be high in high iron waters, but the difficulty of quantifying H_2O_2 in high iron waters (Cooper et al., 2000; King et al., 2007) is a major limitation to this study. As a result, average $\phi_{\text{H}_2\text{O}_{2,\lambda}}$ for arctic surface waters and predictions of photochemical H_2O_2 production are likely an underestimate. This study did not quantify the importance of DOM aromaticity vs. dissolved iron, but given the projected increases in proportion of DOM composition from permafrost soils, this relationship is important to constrain.

In arctic surface waters, the main driver of variability of photochemical H_2O_2 production rates was availability of sunlight. Photochemical H_2O_2 production rates were also limited by CDOM concentration and composition, particularly in the late summer when sunlight availability and CDOM concentrations are at their lowest in arctic surface waters. These results have important implications for increasing CDOM concentrations in North American and European surface waters (De Wit et al., 2021; Monteith et al., 2007; Williamson et al., 2015), and changing sunlight availability in arctic surface waters (Kay & Gettelman, 2009; Šmejkalová et al., 2016). Prior work has predicted that as CDOM concentrations increase in North American and European surface waters, the effect of oxidative stress on microbial communities and composition will increase (Wolf et al., 2018). However, the results from this study show that increasing CDOM concentrations will impact photochemical H_2O_2 production only in waters where H_2O_2 production by CDOM is limited by CDOM concentration. In high CDOM waters, concentrations are high enough to absorb all incoming light, so increases in CDOM concentrations will have no effect on photochemical H_2O_2 production. Therefore, the effect of increasing CDOM concentrations in North American and European surface waters will have varying effects on oxidative stress from H_2O_2 , depending on the water. For example, Williamson et. al 2015 analyzed browning of two lakes in northeastern Pennsylvania, reporting a range of

CDOM concentrations (a_{320} , m^{-1}) that we would expect variable responses of PH_2O_2 to increasing CDOM. The low CDOM (a_{320} , $0.1 - 2.2 m^{-1}$) lake Giles from Williamson et. al 2015 is likely a substrate limited lake with respect to PH_2O_2 , while the higher CDOM (a_{320} , $6 - 18 m^{-1}$) lake Lacawac is likely a light limited lake with respect to PH_2O_2 when its concentrations are high. Thus, the response of PH_2O_2 due to increasing CDOM concentrations would likely be strongest in the substrate limited, low CDOM lake Giles reported in Williamson et. al 2015.

Changes in sunlight availability in arctic surface waters may increase or decrease photochemical H_2O_2 production. Strong light limitation of photochemical H_2O_2 production indicates that changes in light availability will impact photochemical H_2O_2 production independent of whether the water is also substrate limited. Ice-off date in arctic surface waters is happening earlier each year, on average (Šmejkalová et al., 2016). Ice-off in arctic surface waters is typically close to when solar zenith angle is at its peak, thus earlier ice-off increases the number of days that surface waters are exposed to high amounts of light. However, predicted increases in cloud cover on the arctic landscape (Kay & Gettelman, 2009) may decrease photochemical H_2O_2 production. Results from this study show that photochemical H_2O_2 production is highly dependent on both light availability due to seasonal variation in solar zenith angle and daily cloud cover. The results of this study display a strong, linear response of PH_2O_2 to increases or decreases in light availability, and the net-effect of changing light availability depends on the relative importance of increasing cloud cover vs. earlier ice-off date in arctic surface waters.

Furthermore, investigating the limitations of photochemical H_2O_2 production has implications for understanding the shifts in microbial community and composition over the past 20 years in arctic surface waters (Natasha Christman PhD thesis *in prep*). Greater proportions of cyanobacteria in microbial communities in Toolik Lake suggest that the effect of H_2O_2 may be important, given that H_2O_2 may influence cyanobacterial toxic algal blooms in lower latitude freshwaters (Cory et al., 2016; Hellweger et al. 2022). The results from this study propose that concentrations of H_2O_2 are sufficient to exhibit oxidative stress on microbial communities in Toolik Lake. Prior work has also shown differences in microbial community composition in the surface waters vs. bottom waters of Toolik Lake (Crump et al., 2012). The results from this study provide a potential explanation for these differences, given concentrations of H_2O_2 should be high in the surface waters due to photochemical production, and minimal in the bottom waters given that all UV and vis light is absorbed within the top ~ 1 m of Toolik Lake (Cory et al. 2014), and considering that the average depth in Toolik Lake is 7 m. Recent work has shown a strong seasonal pattern in microbial community composition in surface waters of Toolik Lake (Natasha Christman PhD thesis *in prep*). Because photochemical H_2O_2 production varies strongly over the summer season, H_2O_2 may influence microbial community composition. Given that microbial communities decompose DOC to CO_2 in arctic surface waters (Cole et al., 1994; Kling et al., 1991), the production of H_2O_2 may influence this process. Thus, the results from this study provide important insights to the potential role of H_2O_2 in microbial community function and composition, and further work should investigate the response of microbes to H_2O_2 in arctic surface waters directly. The most immediate next step for this research is to quantify concentrations of H_2O_2 in the field to verify predictions of $[H_2O_2]_{ss}$ and PH_2O_2 from this study.

151°W

150°W

149°W

148°W

147°W

146°W

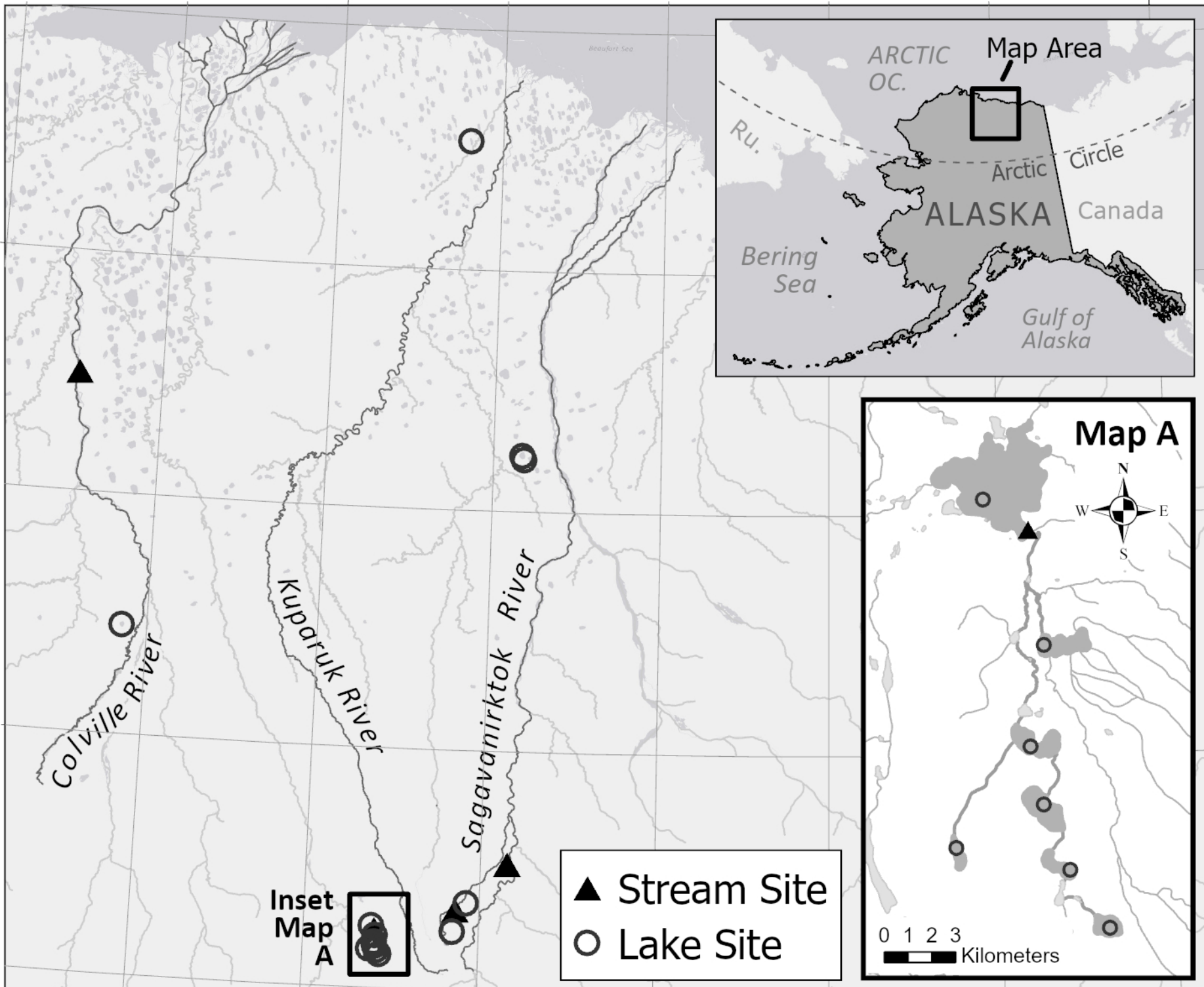
145°W

70°N

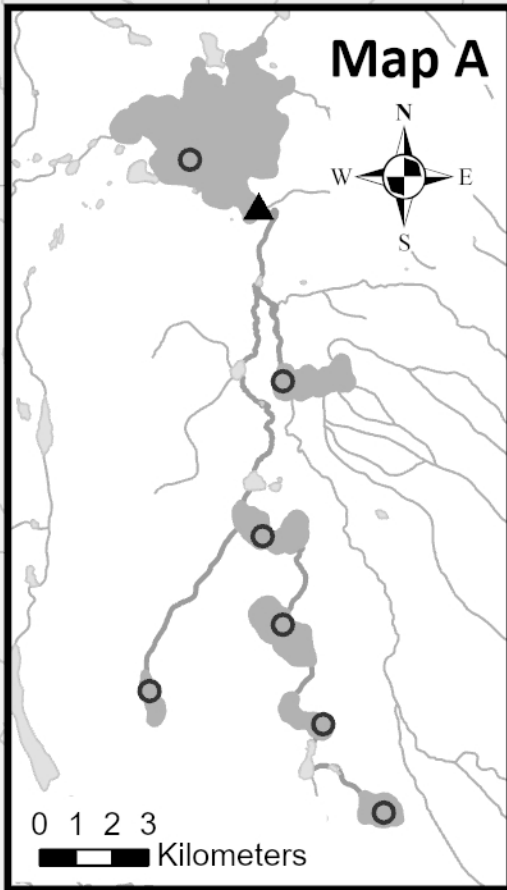
70°N

69°N

69°N



▲ Stream Site
○ Lake Site



Inset Map A

Site	Date Collected	Temperature °C	Specific Conductance (µS/cm)	pH	Fe (µM)	<i>a</i> 305 (m ⁻¹)	Slope Ratio	Fluorescence Index	DOC (µM)	SUVA ₂₅₄	Peak T/A
Toolik Lake	24-Jun-22	5.0	1045	7.4	-	10.6 ± 0.14	1.26 ± 0.02	1.53 ± 0.01	348 ± 4.12	2.48 ± 0.04	0.19 ± 0.02
Toolik Lake	2-Jun-23	1.8	126	7.2	0.19 +/- 0.001	11.9 ± 0.14	1.20 ± 0.02	1.50 ± 0.01	389 ± 4.12	2.56 ± 0.04	0.20 ± 0.02
Toolik Inlet	22-Jun-23	9.3	76.1	7.7	1.05 +/- 0.003	11.2 ± 0.13	0.82 ± 0.02	1.50 ± 0.01	314 ± 2.70	2.81 ± 0.02	0.15 ± 0.02
Toolik Inlet	29-May-23	1.2	48.1	7.1	2.10 +/- 0.003	28.1 ± 0.13	0.85 ± 0.02	1.50 ± 0.01	558 ± 2.70	3.42 ± 0.02	0.21 ± 0.02
I2	20-Jun-23	3.9	27.5	7.5	2.97 ± 0.002	23.7 ± 0.13	1.01 ± 0.02	1.50 ± 0.01	532 ± 3.15	3.34 ± 0.03	0.18 ± 0.02
I4	20-Jun-23	7.3	23.9	6.8	3.62 ± 0.002	22.1 ± 0.13	1.02 ± 0.02	1.48 ± 0.01	475 ± 3.15	3.38 ± 0.03	0.15 ± 0.02
I5	20-Jun-23	4.5	22.4	6.6	1.58 ± 0.002	21.1 ± 0.13	1.07 ± 0.02	1.48 ± 0.01	504 ± 3.15	3.13 ± 0.03	0.19 ± 0.02
I6 HW	21-Jun-23	7.5	98.8	7.4	0.37 ± 0.002	14.8 ± 0.13	1.25 ± 0.02	1.45 ± 0.01	371 ± 3.15	3.07 ± 0.03	0.20 ± 0.02
I6	21-Jun-23	4.1	46.3	7.5	0.92 ± 0.002	19.7 ± 0.13	1.08 ± 0.02	1.49 ± 0.01	475 ± 3.15	3.11 ± 0.03	0.15 ± 0.02
I8	21-Jun-23	7.2	67.6	7.7	2.24 ± 0.002	21.1 ± 0.13	0.98 ± 0.02	1.50 ± 0.01	408 ± 3.15	3.60 ± 0.03	0.15 ± 0.02
LHS 2-01	8-Jul-23	20.7	91.8	7.5	6.36 ± 0.002	29.8 ± 0.07	1.08 ± 0.02	1.50 ± 0.01	809 ± 3.15	2.90 ± 0.03	0.19 ± 0.02
LHS 2-01	27-Jul-23	21.6	103	7.7	6.47 ± 0.002	39.9 ± 0.07	1.01 ± 0.02	1.50 ± 0.01	958 ± 3.15	3.26 ± 0.03	0.17 ± 0.02
LS 1-05	8-Jul-23	15.5	226	8.2	0.84 ± 0.002	10.0 ± 0.07	1.34 ± 0.02	1.41 ± 0.01	624 ± 3.15	1.61 ± 0.03	0.36 ± 0.02
LS 1-05	27-Jul-23	17.6	345	8.1	0.80 ± 0.002	13.1 ± 0.07	1.34 ± 0.02	1.46 ± 0.01	734 ± 3.15	1.78 ± 0.03	0.30 ± 0.02
LS 1-27	8-Jul-22	19.9	175	8.1	0.34 ± 0.002	5.91 ± 0.07	1.89 ± 0.02	1.55 ± 0.01	274 ± 3.15	1.86 ± 0.03	0.33 ± 0.02
LS 1-28	8-Jul-22	20.3	160	8.5	0.76 ± 0.002	18.0 ± 0.07	1.33 ± 0.02	1.53 ± 0.01	676 ± 3.15	2.35 ± 0.03	0.23 ± 0.02
LHS 2-03	27-Jul-23	18.7	216	7.8	0.40 ± 0.002	12.2 ± 0.07	0.94 ± 0.02	1.54 ± 0.01	330 ± 3.15	2.89 ± 0.03	0.12 ± 0.02
Oksrukuyik Creek	7-Jun-23	5.8	31.3	6.9	1.72 ± 0.002	25.6 ± 0.11	0.89 ± 0.02	1.47 ± 0.01	508 ± 2.55	3.50 ± 0.02	0.14 ± 0.02
Sagavanirktok River	8-Jun-22	3.3	216	6.5	-	5.18 ± 0.13	1.21 ± 0.02	1.52 ± 0.01	122 ± 3.15	2.87 ± 0.03	0.20 ± 0.02
LTER 345	27-Jun-23	7.4	199	7.0	0.17 ± 0.002	9.37 ± 0.13	1.13 ± 0.02	1.47 ± 0.01	318 ± 3.15	2.61 ± 0.03	0.21 ± 0.02
Fog 01	5-Jul-23	14.3	157	7.8	0.11 ± 0.002	8.44 ± 0.13	1.42 ± 0.02	1.41 ± 0.01	339 ± 3.15	2.31 ± 0.03	0.24 ± 0.02

Table 1: Surface water temperature, specific conductance, pH, total dissolved iron, DOC concentration, and proxies for DOM composition collected to quantify the $\phi_{\text{H}_2\text{O}_{2,\lambda}}$ in the spring/summer months of May-July of 2022 & 2023. Analytical error reported in the text and in this table for Fe, *a*305, Slope ratio, fluorescence index, DOC, SUVA₂₅₄, and Peak T/A for all sites excluding Toolik Lake, Toolik Inlet, and Oksrukuyik Creek are based on average standard error of field duplicates from a dataset from summer 2023. Toolik Lake, Toolik Inlet, and Oksrukuyik contained sufficient numbers of field duplicate data to report analytical error unique to each of those sites, respectively.

Site	Date Collected	$\phi_{\text{H}_2\text{O}_2,275}$	$\phi_{\text{H}_2\text{O}_2,305}$	$\phi_{\text{H}_2\text{O}_2,365}$	$\phi_{\text{H}_2\text{O}_2,385}$	$\phi_{\text{H}_2\text{O}_2,405}$	c	95 % CI	d	95% CI
Toolik Lake	24-Jun-22	2.11 ± 0.02	1.28 ± 0.01	0.35 ± 0.004	0.35 ± 0.06	0.30 ± 0.04	0.2264	0.1191 - 0.3338	-0.017	-0.01863 - 0.01536
Toolik Lake	2-Jun-23	2.06 ± 0.04	1.08 ± 0.04	0.28 ± 0.01	0.22 ± 0.01	0.17 ± 0.01	0.6548	0.4228 - 0.8868	-0.02096	-0.0222 - 0.01971
Toolik Inlet	22-Jun-23	1.96 ± 0.11	1.25 ± 0.02	0.29 ± 0.01	0.23 ± 0.02	0.15 ± 0.01	0.3292	0.1046 - 0.5539	-0.01856	-0.02093 - 0.01618
Toolik Inlet	29-May-23	6.68 ± 0.94	3.28 ± 0.04	0.91 ± 0.02	0.73 ± 0.01	0.58 ± 0.01	2.45	-1.452 - 6.352	-0.02151	-0.02711 - 0.01592
12	20-Jun-23	2.96 ± 0.16	1.37 ± 0.02	0.41 ± 0.02	0.32 ± 0.002	0.24 ± 0.01	1.384	0.2763 - 2.493	-0.0224	-0.02522 - 0.01958
14	20-Jun-23	3.07 ± 0.04	1.69 ± 0.04	0.54 ± 0.001	0.46 ± 0.02	0.33 ± 0.02	0.4801	0.3427 - 0.6175	-0.0184	-0.0194 - 0.01741
15	20-Jun-23	2.53 ± 0.12	1.35 ± 0.08	0.42 ± 0.01	0.38 ± 0.01	0.33 ± 0.02	0.4173	0.136 - 0.6985	-0.0186	-0.02095 - 0.01626
16 HW	21-Jun-23	3.2 ± 0.07	1.97 ± 0.05	0.66 ± 0.01	0.48 ± 0.003	0.31 ± 0.01	0.4063	0.3117 - 0.5009	-0.01751	-0.01832 - 0.01671
16	21-Jun-23	2.63 ± 0.05	1.40 ± 0.04	0.43 ± 0.01	0.43 ± 0.02	0.29 ± 0.01	0.4258	0.2364 - 0.6151	-0.01855	-0.02009 - 0.017
18	21-Jun-23	4.18 ± 0.12	2.07 ± 0.04	0.63 ± 0.01	0.51 ± 0.03	0.40 ± 0.01	1.217	0.5991 - 1.835	-0.02068	-0.02246 - 0.0189
LHS 2-01	8-Jul-22	2.57 ± 0.36	1.19 ± 0.03	0.28 ± 0.01	0.31 ± 0.01	0.21 ± 0.02	1.421	-1.127 - 3.97	-0.02301	-0.02933 - 0.01668
LHS 2-01	27-Jul-23	6.39 ± 0.64	3.06 ± 0.08	0.38 ± 0.01	0.28 ± 0.02	0.14 ± 0.01	9.277	-5.115 - 23.67	-0.02645	-0.03196 - 0.02094
LS 1-05	8-Jul-22	2.13 ± 0.03	1.15 ± 0.08	0.23 ± 0.01	0.23 ± 0.004	0.17 ± 0.01	0.7175	0.3186 - 1.116	-0.02114	-0.0231 - 0.01919
LS 1-05	27-Jul-23	2.43 ± 0.02	1.08 ± 0.01	0.25 ± 0.01	0.20 ± 0.003	0.16 ± 0.01	2.338	1.318 - 3.358	-0.025	-0.02655 - 0.02346
LS 1-27	8-Jul-22	1.98 ± 0.06	1.02 ± 0.03	0.15 ± 0.01	0.19 ± 0.01	0.12 ± 0.01	1.081	0.3914 - 1.77	-0.02291	-0.02516 - 0.02066
LS 1-28	8-Jul-22	2.39 ± 0.15	1.27 ± 0.05	0.18 ± 0.01	0.16 ± 0.01	0.11 ± 0.01	1.047	0.06441 - 2.03	-0.02212	-0.02542 - 0.01882
LHS 2-03	27-Jul-23	2.72 ± 0.12	1.42 ± 0.03	0.41 ± 0.01	0.34 ± 0.01	0.28 ± 0.02	0.6585	0.3014 - 1.016	-0.01999	-0.02189 - 0.01809
Oksrukuyik Creek	7-Jun-23	3.17 ± 0.15	1.81 ± 0.17	0.56 ± 0.01	0.47 ± 0.01	0.35 ± 0.02	0.4722	0.1633 - 0.7811	-0.0182	-0.02047 - 0.01593
Sagavanirktok River	8-Jun-22	1.66 ± 0.04	0.93 ± 0.03	0.20 ± 0.01	0.16 ± 0.02	0.10 ± 0.0006	0.4788	0.2524 - 0.7052	-0.02058	-0.02224 - 0.01892
LTER 345	27-Jun-23	1.72 ± 0.03	0.84 ± 0.02	0.15 ± 0.003	0.11 ± 0.001	0.07 ± 0.0007	1.535	0.9958 - 2.075	-0.02469	-0.02593 - 0.02344
Fog 01	5-Jul-23	2.17 ± 0.02	1.01 ± 0.02	0.25 ± 0.01	0.16 ± 0.01	0.16 ± 0.01	1.561	0.9411 - 2.18	-0.02395	-0.02535 - 0.02254

Table 2: Apparent quantum yields for hydrogen peroxide from CDOM ($\phi_{\text{H}_2\text{O}_2,\lambda}$), represented in mmol H_2O_2 mol photon⁻¹ at each wavelength $\phi_{\text{H}_2\text{O}_2,\lambda}$ was measured. Values at each wavelength are reported as the average ± 1 SE of experimental replicates (n=3). Best-fit parameters c and d (see Equation 3) for the $\phi_{\text{H}_2\text{O}_2,\lambda}$ generated by Matlab curve fitting application, with 95% confidence intervals for each parameter.

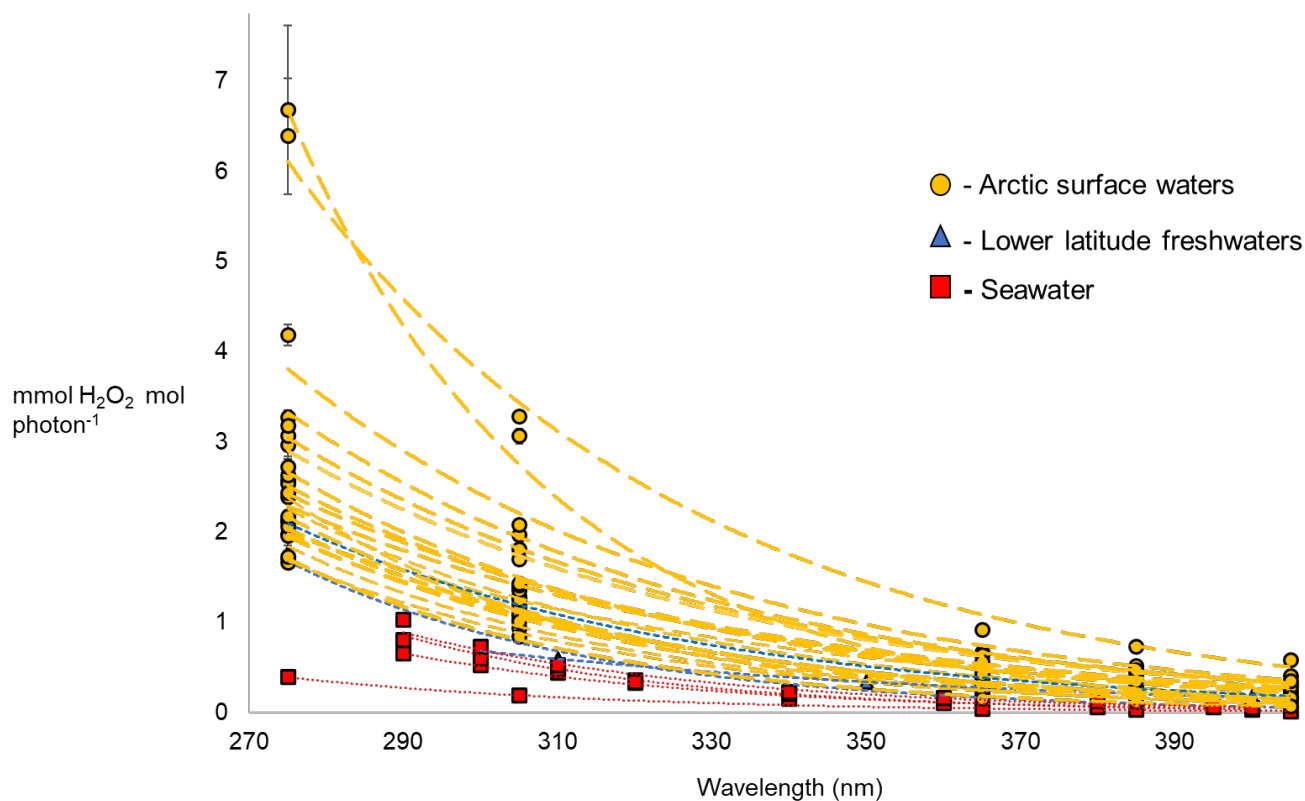


Figure 2: H₂O₂ apparent quantum yield spectra ($\phi_{\text{H}_2\text{O}_2,\lambda}$) plotted as a function of wavelength. $\phi_{\text{H}_2\text{O}_2,\lambda}$ decrease exponentially with increasing wavelength. $\phi_{\text{H}_2\text{O}_2,\lambda}$ for arctic surface waters in this study (yellow) are reported as average \pm 1 SE experimental replicates (n = 3). Literature $\phi_{\text{H}_2\text{O}_2,\lambda}$ values for freshwater and seawater plotted in blue and red, respectively.

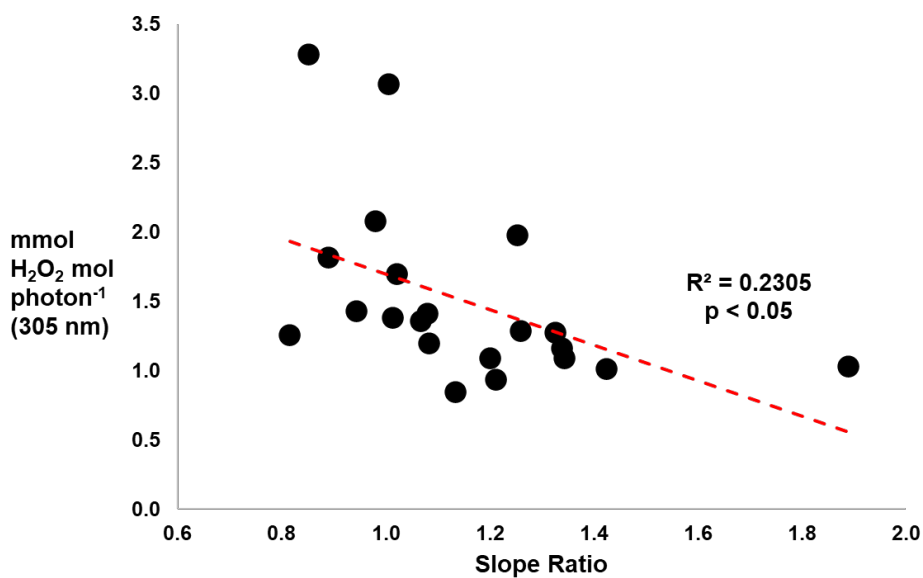
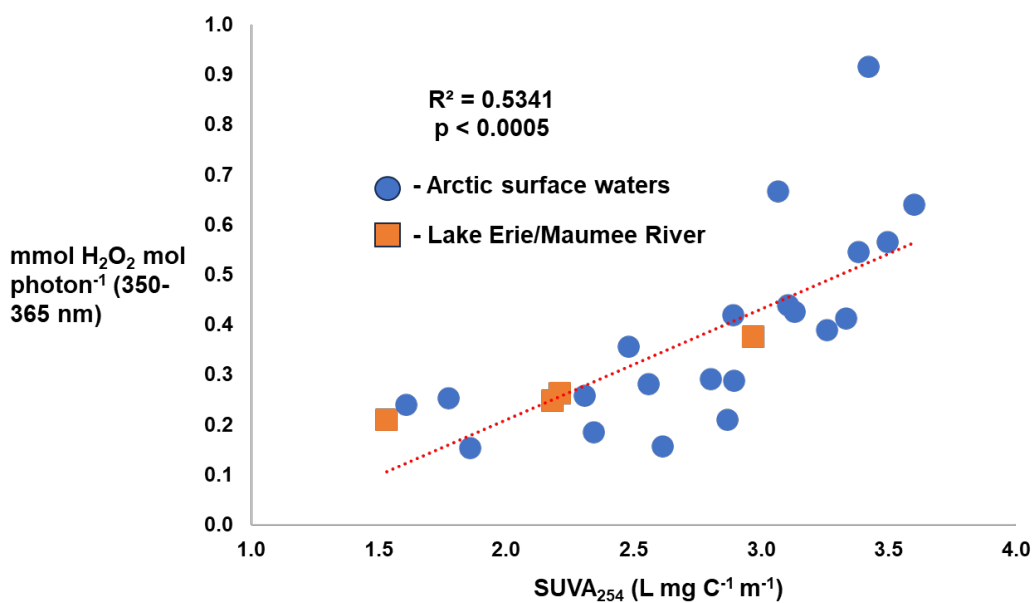


Figure 3a: H₂O₂ apparent quantum yield spectra at 305 nm ($\phi_{\text{H}_2\text{O}_2,305}$) plotted as a function of spectral slope ratio (S_R). Data were fit using a linear least squares regression ($y = -1.281x + 2.978$) in Microsoft Excel, where $R^2 = 0.2305$ and $p < 0.05$.

Figure 3b: H₂O₂ apparent quantum yield spectra at 365 nm for this study and 350 nm for Pandey et. al 2022 ($\phi_{\text{H}_2\text{O}_2,350-365}$) plotted as a function of $SUVA_{254}$. Data were fit using a linear least squares regression ($y = 0.2216x - 0.2342$) in Microsoft Excel, where $R^2 = 0.5341$ and $p < 0.0005$.



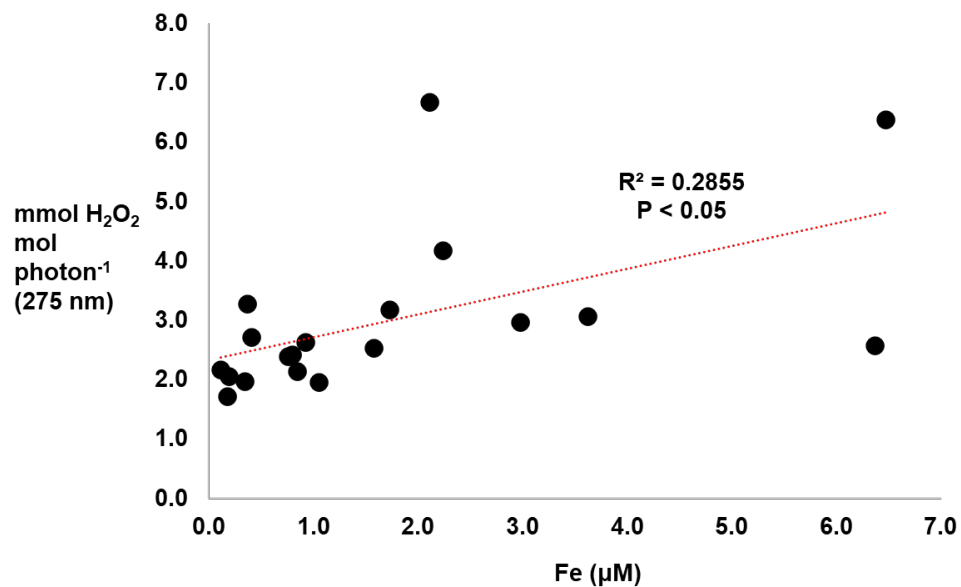


Figure 4: H₂O₂ apparent quantum yield spectra at 275 nm ($\phi_{\text{H}_2\text{O}_2,275}$) plotted as a function of total dissolved iron concentrations in arctic surface waters from this study. Data were fit using a linear least squares regression ($y = 0.382x + 2.339$) in Microsoft Excel, where $R^2 = 0.286$ and $p < 0.05$.

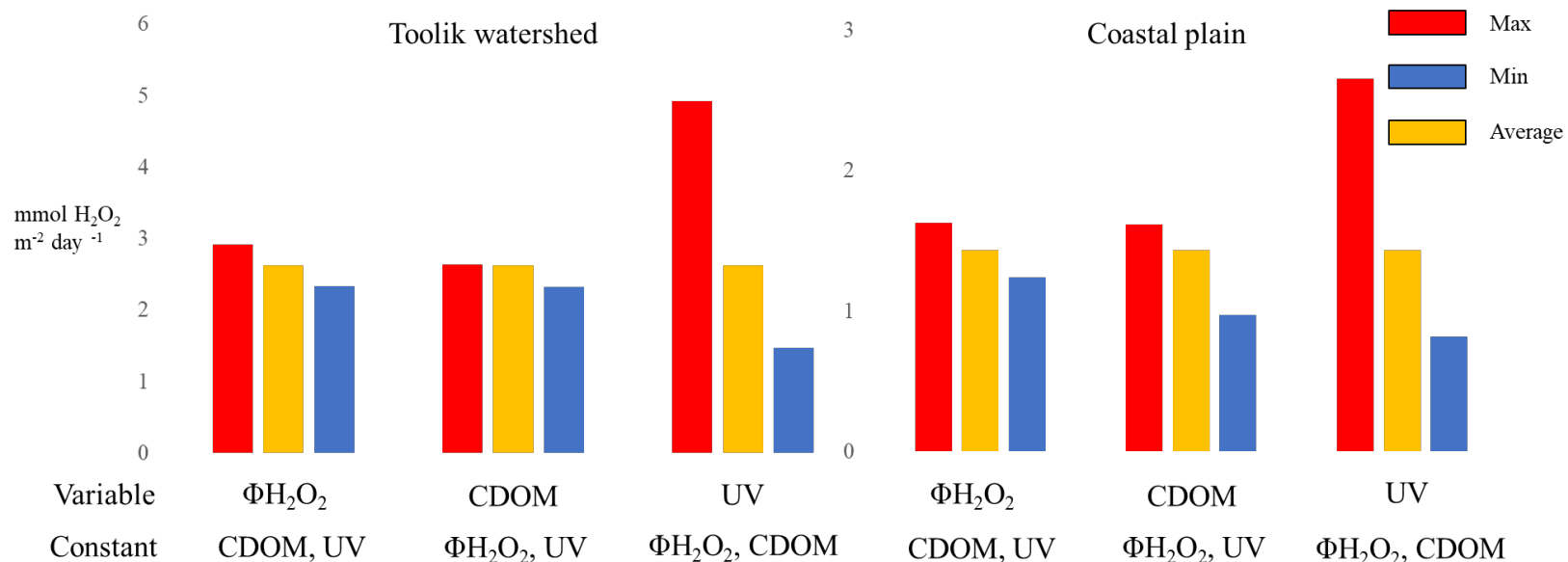


Figure 5: Effect of CDOM, photon flux, and $\phi_{H_2O_2, \lambda}$ on photochemical H_2O_2 production rates (PH_2O_2). For both groupings of sites, PH_2O_2 was calculated as in Equation 4 by holding two variables constant at the average and varying one across its minimum to maximum observed range of values.

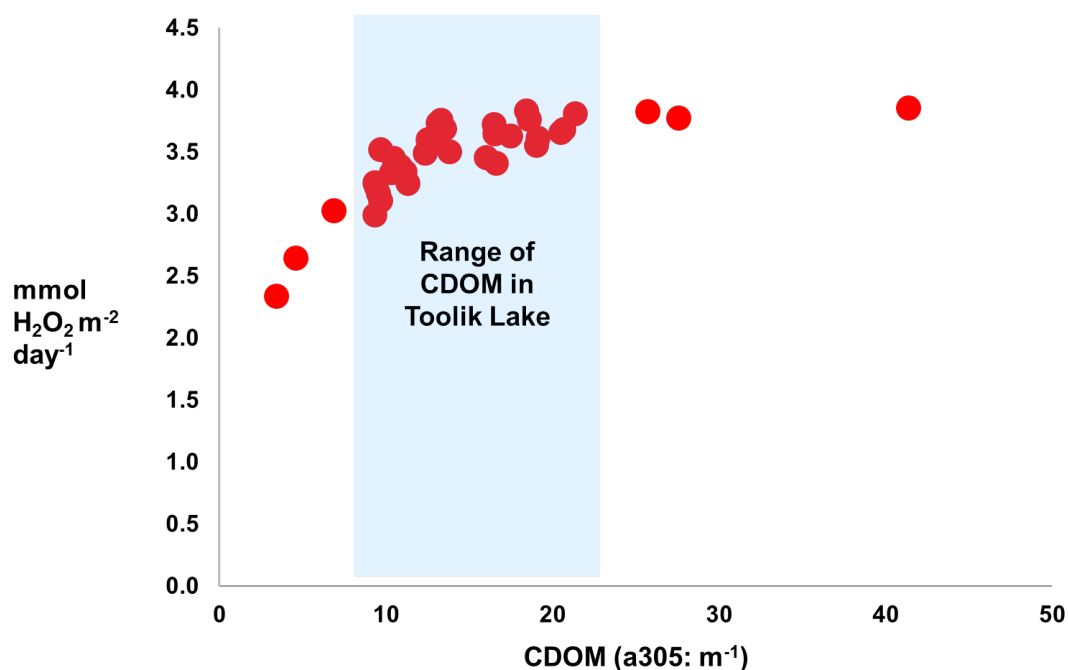


Figure 6: Non-linear response of photochemical H_2O_2 production rates (PH_2O_2) across a range of CDOM concentrations in Toolik Lake. Points within the shaded area represent the expected range of CDOM concentrations in Toolik Lake. Points outside the shaded area were scaled from the average a_{305} for Toolik Lake by factors of 1.5, 2, and 3 in both directions, respectively.

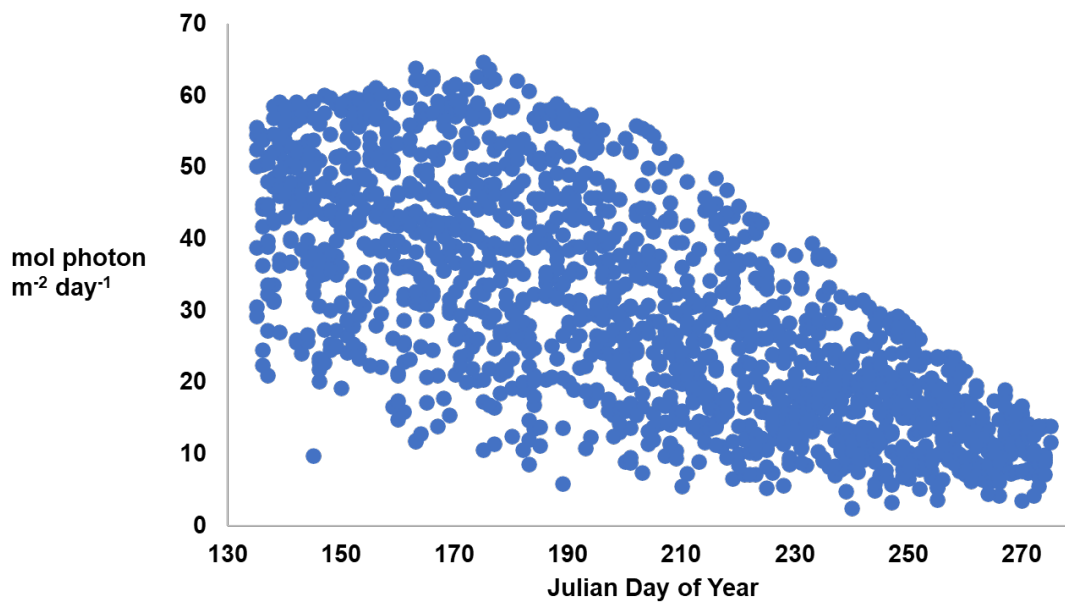


Figure S1: Daily photon fluxes recorded at Toolik Field Station from May to October from the period 2012-2023. Photon fluxes are reported as the sum of mol photons m⁻² day⁻¹ from the UV to visible wavelength spectrum (280-600 nm).

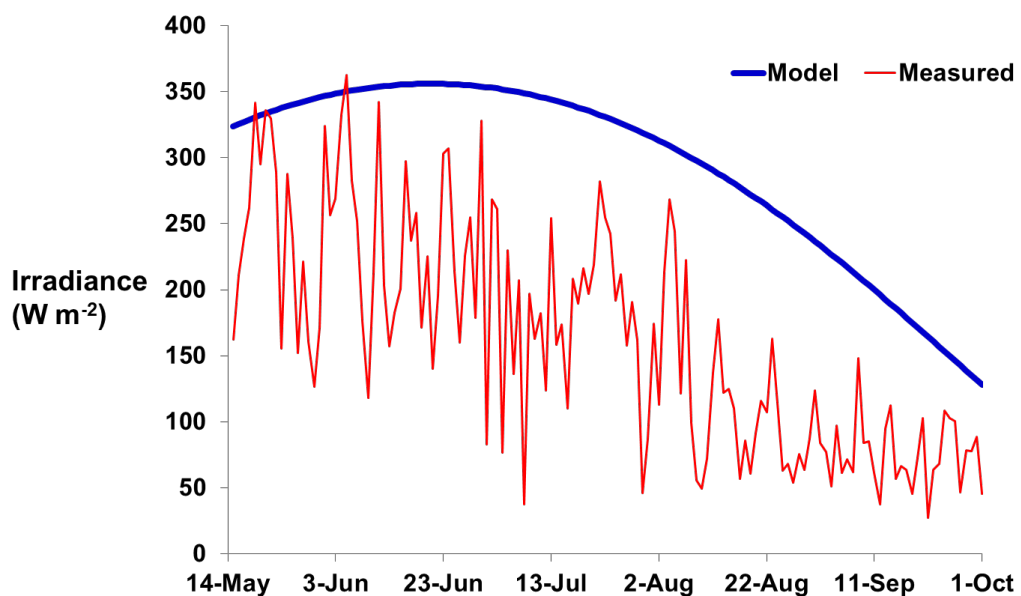


Figure S2: Daily mean measured and modeled irradiance for Toolik Field Station used to calculate cloudiness factor F plotted from May-October in 2023. Similar results were observed in all years, thus years 2012-2022 are not shown.

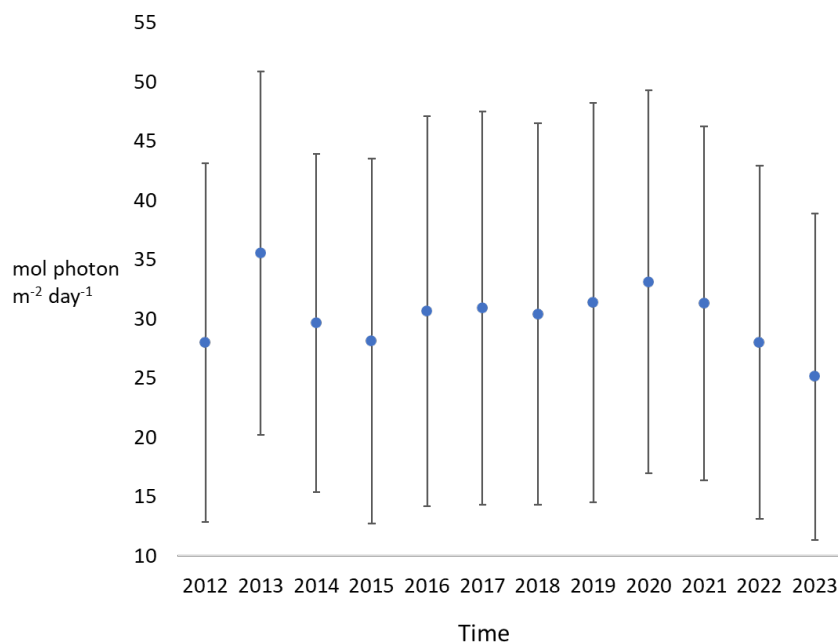


Figure S3: Summer (May-October) mean photon fluxes measured at Toolik Field Station from the period 2012-2023. Points reported are average photon fluxes for the whole summer ± 1 standard deviation ($n = 98 - 137$, with n varying by year). Photon fluxes are reported as a sum of mol photons $m^{-2} day^{-1}$ from UV and visible wavelengths (280-600 nm).

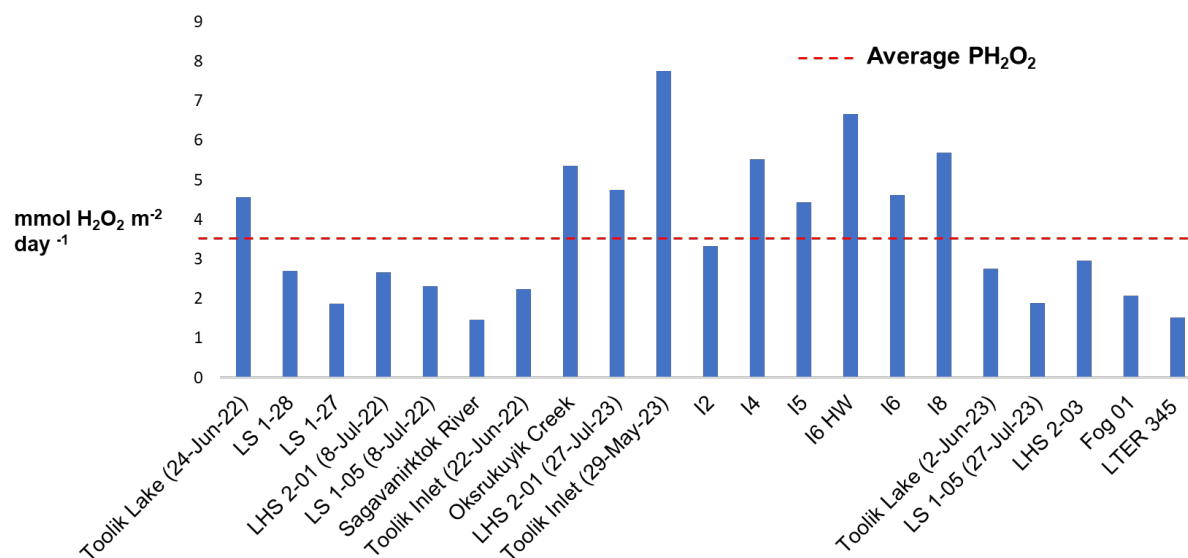


Figure S4: Photochemical H₂O₂ production rates (PH₂O₂) calculated as in [Equation 4](#) for all waters in this study. Photon fluxes at peak zenith angle (solstice), CDOM concentration from date of sample collection, and the $\phi_{H_2O_2,\lambda}$ measured in this study were used to calculate PH₂O₂ in each water.

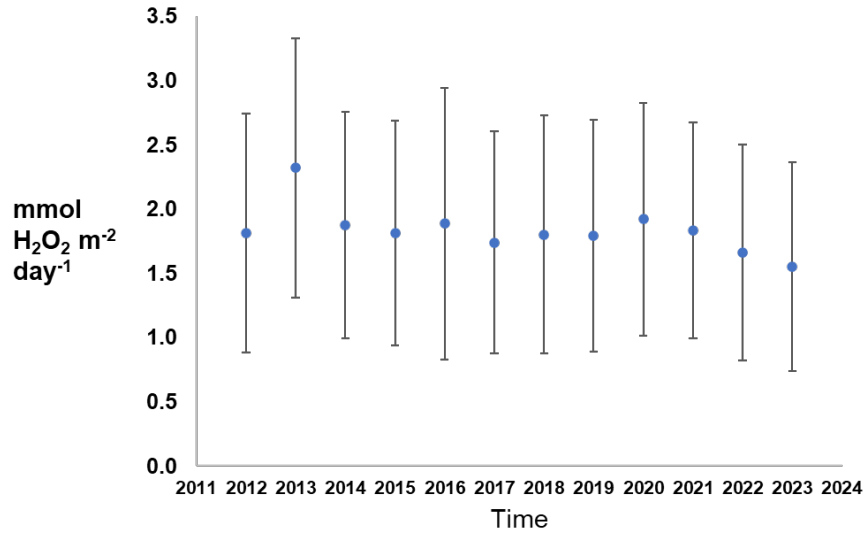


Figure S5a: Yearly mean daily PH₂O₂ in Toolik Lake calculated for every summer (May-October) from the period 2012-2023 as in [Equation 4](#). Photon fluxes for each day, average CDOM concentrations in Toolik Lake for each month of each year, and the $\phi_{\text{H}_2\text{O}_2, \lambda}$ measured in this study for Toolik Lake were used to calculate PH₂O₂. Points represent the average daily PH₂O₂ for each year ± 1 standard deviation ($n = 98 - 137$, with n varying each year).

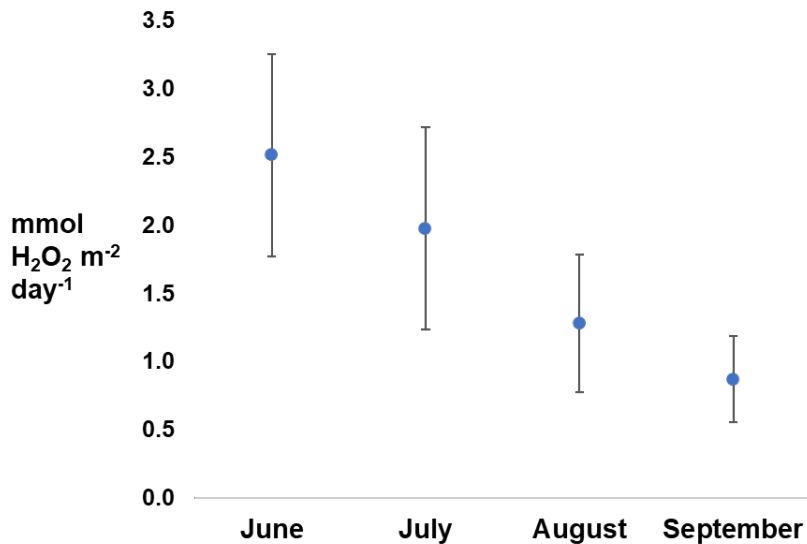


Figure S5b: Monthly mean daily PH₂O₂ was calculated as in Figure S5a, but daily PH₂O₂ was averaged for each month over the period 2012-2023 during ice-free months. Points represent average daily PH₂O₂ for each month across years 2012-2023 ± 1 standard deviation ($n = 296 - 370$, with n varying for each month).

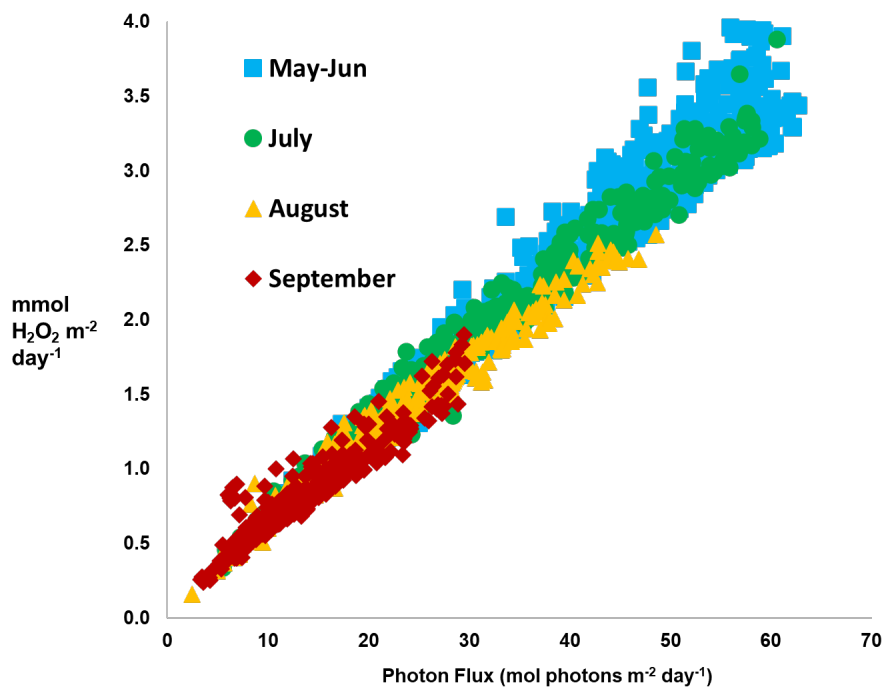


Figure S6: Daily PH_2O_2 in Toolik Lake from years 2012-2023 plotted as a function of daily photon flux. Points are grouped by time of year. Photon fluxes are reported as a sum of mol photons $\text{m}^{-2} \text{ day}^{-1}$ from UV and visible wavelengths (280-600 nm).

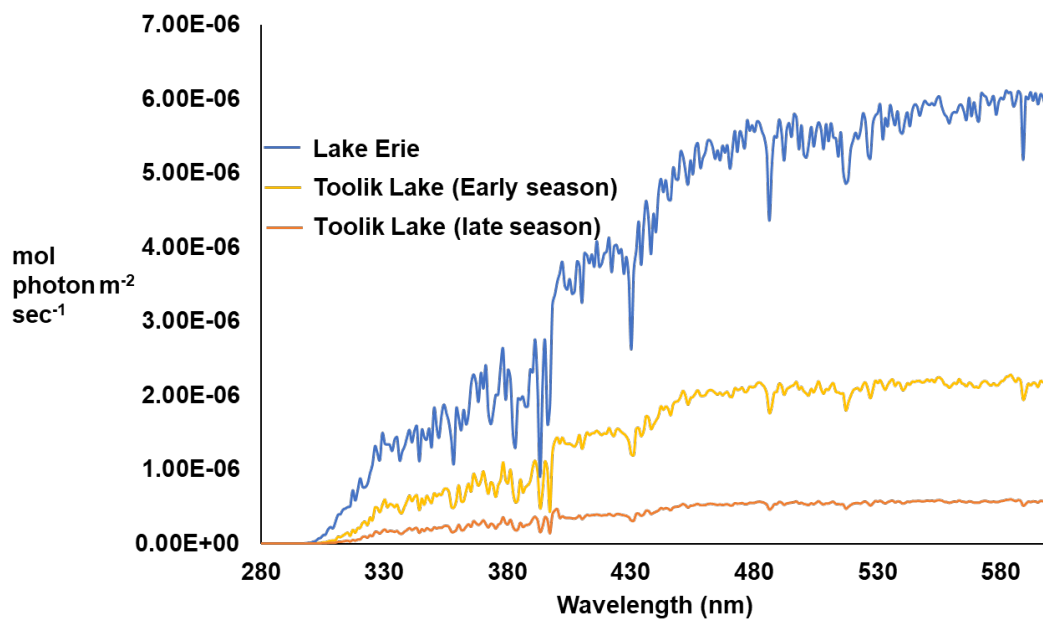


Figure S7: Photon flux spectra plotted as a function of wavelength from the UV to visible range of light (280-600 nm). Photon fluxes for Lake Erie, early season Toolik lake, and late season Toolik Lake plotted to show the difference of incoming sunlight at higher latitudes due to solar zenith angle.

References

- Andrews, S. S., Caron, S., & Zafiriou, O. C. (2000). *Photochemical Oxygen Consumption in Marine Waters: A Major Sink for Colored Dissolved Organic Matter?* (Vol. 45, Issue 2). <https://about.jstor.org/terms>
- Bowen, J. C., Ward, C. P., Kling, G. W., & Cory, R. M. (2020). Arctic Amplification of Global Warming Strengthened by Sunlight Oxidation of Permafrost Carbon to CO₂. *Geophysical Research Letters*, 47(12). <https://doi.org/10.1029/2020GL087085>
- Cole, J. J., Caraco, N. F., Kling, G. W., Kratz, T. K., Sowers, T., Bender, M., Raynaud, D., Korotke-, Y. S., Cole, J. J., Caraco, N. F., Kling, G. W., & Kratz, T. K. (1994). Carbon Dioxide Supersaturation in the Surface Waters of Lakes. In *J. Geol. Soc. London* (Vol. 6). <https://www.science.org>
- Cooper, W. J., Lean, D. R. S., & Carey, J. H. (n.d.). *and Temporal Patterns of Hydrogen Peroxide in Lake Waters*.
- Cooper, W. J., Moegling, J. K., Kieber, R. J., & Kiddle, J. J. (2000). A chemiluminescence method for the analysis of H₂O₂ in natural waters. In *Marine Chemistry* (Vol. 70). www.elsevier.nl/locate/marchem
- Cooper, W. J., Shao, C., S Lean, D. R., Gordon, A. S., & Scully, F. E. (1994). *Factors Affecting the Distribution of H₂O₂ in Surface Waters* (Vol. 18). UTC. <https://pubs.acs.org/sharingguidelines>
- Cooper, W. J., Zilka, R. G., Petasne, R. G., & Plane, J. M. C. (1988). Photochemical Formation of H₂O₂ in Natural Waters Exposed to Sunlight. In *Environ. Sel. Technol* (Vol. 22). <https://pubs.acs.org/sharingguidelines>
- Cory, R. M., Crump, B. C., Dobkowski, J. A., & Kling, G. W. (2013). Surface exposure to sunlight stimulates CO₂ release from permafrost soil carbon in the Arctic. *Proceedings of the National Academy of Sciences of the United States of America*, 110(9), 3429–3434. <https://doi.org/10.1073/pnas.1214104110>
- Cory, R. M., Davis, T. W., Dick, G. J., Johengen, T., Deneff, V. J., Berry, M. A., Page, S. E., Watson, S. B., Yuhas, K., & Kling, G. W. (2016). Seasonal dynamics in dissolved organic matter, hydrogen peroxide, and cyanobacterial blooms in Lake Erie. *Frontiers in Marine Science*, 3(APR). <https://doi.org/10.3389/fmars.2016.00054>
- Cory, R. M., Harrold, K. H., Neilson, B. T., & Kling, G. W. (2015). Controls on dissolved organic matter (DOM) degradation in a headwater stream: The influence of photochemical and hydrological conditions in determining light-limitation or substrate-limitation of photo-degradation. *Biogeosciences*, 12(22), 6669–6685. <https://doi.org/10.5194/bg-12-6669-2015>
- Cory, R. M., McKnight, D. M., Chin, Y. P., Miller, P., & Jaros, C. L. (2007). Chemical characteristics of fulvic acids from Arctic surface waters: Microbial contributions and

- photochemical transformations. *Journal of Geophysical Research: Biogeosciences*, 112(4). <https://doi.org/10.1029/2006JG000343>
- Cory, R. M., McNeill, K., Cotner, J. P., Amado, A., Purcell, J. M., & Marshall, A. G. (2010). Singlet oxygen in the coupled photochemical and biochemical oxidation of dissolved organic matter. *Environmental Science and Technology*, 44(10), 3683–3689. <https://doi.org/10.1021/es902989y>
- Cory, R. M., Miller, M. P., Mcknight, D. M., Guerard, J. J., & Miller, P. L. (2010). Effect of instrument-specific response on the analysis of fulvic acid fluorescence spectra. *Limnology and Oceanography: Methods*, 8(2), 67–78. <https://doi.org/10.4319/lom.2010.8.67>
- Cory, R., Ward, C., Crump, B., & Kling, G. (2014). Sunlight controls water column processing of carbon in arctic fresh waters. *Science*, 345(6199), 925–928.
- Crump, B. C., Amaral-Zettler, L. A., & Kling, G. W. (2012). Microbial diversity in arctic freshwaters is structured by inoculation of microbes from soils. *ISME Journal*, 6(9), 1629–1639. <https://doi.org/10.1038/ismej.2012.9>
- De Wit, H. A., Stoddard, J. L., Monteith, D. T., Sample, J. E., Austnes, K., Couture, S., Fölster, J., Higgins, S. N., Houle, D., Hruška, J., Krám, P., Kopáček, J., Paterson, A. M., Valinia, S., Van Dam, H., Vuorenmaa, J., & Evans, C. D. (2021). Cleaner air reveals growing influence of climate on dissolved organic carbon trends in northern headwaters. *Environmental Research Letters*, 16(10). <https://doi.org/10.1088/1748-9326/ac2526>
- Drábková, M., Admiraal, W., & Maršálek, B. (2007). Combined exposure to hydrogen peroxide and light-selective effects on cyanobacteria, green algae, and diatoms. *Environmental Science and Technology*, 41(1), 309–314. <https://doi.org/10.1021/es060746i>
- Feng, X., Vonk, J. E., Van Dongen, B. E., Gustafsson, Ö., Semiletov, I. P., Dudarev, O. V., Wang, Z., Montluçon, D. B., Wacker, L., & Eglinton, T. I. (2013). Differential mobilization of terrestrial carbon pools in Eurasian Arctic river basins. *Proceedings of the National Academy of Sciences of the United States of America*, 110(35), 14168–14173. <https://doi.org/10.1073/pnas.1307031110>
- Gareis, J. A. L., Lesack, L. F. W., & Bothwell, M. L. (2010). Attenuation of in situ UV radiation in Mackenzie Delta lakes with varying dissolved organic matter compositions. *Water Resources Research*, 46(9). <https://doi.org/10.1029/2009WR008747>
- Haber, F., Weiss, J., Sesh, J. O., & Eiss, W. (n.d.). *The Catalytic Decomposition of Hydrogen Peroxide by Iron Salts* By F r i t z H aber and*. <https://royalsocietypublishing.org/>
- Häkkinen, P. J., Anesio, A. M., & Granéli, W. (2004). Hydrogen peroxide distribution, production, and decay in boreal lakes. *Canadian Journal of Fisheries and Aquatic Sciences*, 61(8), 1520–1527. <https://doi.org/10.1139/F04-098>

- Hammerschmidt, C. R., & Fitzgerald, W. F. (2010). Iron-mediated photochemical decomposition of methylmercury in an arctic Alaskan Lake. *Environmental Science and Technology*, 44(16), 6138–6143. <https://doi.org/10.1021/es1006934>
- Hellweger, F. L., Martin, R. M., Eigemann, F., Smith, D. J., Dick, G. J., & Wilhelm, S. W. (n.d.). *Models predict planned phosphorus load reduction will make Lake Erie more toxic*. <https://www.science.org>
- Helms, J. R., Stubbins, A., Ritchie, J. D., Minor, E. C., Kieber, D. J., & Mopper, K. (2008). Absorption spectral slopes and slope ratios as indicators of molecular weight, source, and photobleaching of chromophoric dissolved organic matter. *Limnology and Oceanography*, 53(3), 955–969. <https://doi.org/10.4319/lo.2008.53.3.0955>
- J H Festos, B. H. (n.d.). *OXIDATION OF TARTARIC ACID IN PRESEXCE OF IRON. 899 LXXZII.-Oxictutioiz of Tcxriaric Acid iia prcsezce of Jrolz*.
- Jerome, J. H., & Bukata, R. P. (1998). Impact of stratospheric ozone depletion on photoproduction of hydrogen peroxide in Lake Ontario. *Journal of Great Lakes Research*, 24(4), 929–935. [https://doi.org/10.1016/S0380-1330\(98\)70873-1](https://doi.org/10.1016/S0380-1330(98)70873-1)
- Kay, J. E., & Gettelman, A. (2009). Cloud influence on and response to seasonal Arctic sea ice loss. *Journal of Geophysical Research Atmospheres*, 114(18). <https://doi.org/10.1029/2009JD011773>
- Keller, K., Blum, J. D., & Kling, G. W. (2007). Geochemistry of soils and streams on surfaces of varying ages in arctic Alaska. *Arctic, Antarctic, and Alpine Research*, 39(1), 84–98. [https://doi.org/10.1657/1523-0430\(2007\)39\[84:GOSASO\]2.0.CO;2](https://doi.org/10.1657/1523-0430(2007)39[84:GOSASO]2.0.CO;2)
- Kieber, D. J., Miller, G. W., Neale, P. J., & Mopper, K. (2014). Wavelength and temperature-dependent apparent quantum yields for photochemical formation of hydrogen peroxide in seawater. *Environmental Sciences: Processes and Impacts*, 16(4), 777–791. <https://doi.org/10.1039/c4em00036f>
- King, D. W., Cooper, W. J., Rusak, S. A., Peake, B. M., Kiddle, J. J., O'Sullivan, D. W., Melamed, M. L., Morgan, C. R., & Theberge, S. M. (2007). Flow injection analysis of H₂O₂ in natural waters using acridinium ester chemiluminescence: Method development and optimization using a kinetic model. *Analytical Chemistry*, 79(11), 4169–4176. <https://doi.org/10.1021/ac062228w>
- Kling, G., Kipphut, G., & Miller, M. (1991). Arctic Lakes and Streams as Gas Conduits to the Atmosphere: Implications for Tundra Carbon Budgets. *Science*, 251(4991), 298–301.
- Kling, G. W., Kipphut, G. W., Miller, M. M., & O'Brien, W. J. (2000). Integration of lakes and streams in a landscape perspective: The importance of material processing on spatial patterns and temporal coherence. *Freshwater Biology*, 43(3), 477–497. <https://doi.org/10.1046/j.1365-2427.2000.00515.x>

- Latifi, A., Ruiz, M., & Zhang, C. C. (2009). Oxidative stress in cyanobacteria. In *FEMS Microbiology Reviews* (Vol. 33, Issue 2, pp. 258–278). Blackwell Publishing Ltd. <https://doi.org/10.1111/j.1574-6976.2008.00134.x>
- Lesser, M. P. (2006). Oxidative stress in marine environments: Biochemistry and physiological ecology. In *Annual Review of Physiology* (Vol. 68, pp. 253–278). <https://doi.org/10.1146/annurev.physiol.68.040104.110001>
- Leunert, F., Eckert, W., Paul, A., Gerhardt, V., & Grossart, H. P. (2014). Phytoplankton response to UV-generated hydrogen peroxide from natural organic matter. *Journal of Plankton Research*, 36(1), 185–197. <https://doi.org/10.1093/plankt/fbt096>
- Marsico, R. M., Schneider, R. J., Voelker, B. M., Zhang, T., Diaz, J. M., Hansel, C. M., & Ushijima, S. (2015). Spatial and temporal variability of widespread dark production and decay of hydrogen peroxide in freshwater. *Aquatic Sciences*, 77(4), 523–533. <https://doi.org/10.1007/s00027-015-0399-2>
- McKnight, D. M., Boyer, E. W., Westerhoff, P. K., Doran, P. T., Kulbe, T., & Andersen, D. T. (2001). Spectrofluorometric characterization of dissolved organic matter for indication of precursor organic material and aromaticity. *Limnology and Oceanography*, 46(1), 38–48. <https://doi.org/10.4319/lo.2001.46.1.0038>
- Michaelson, G. J., Ping, C. L., Kling, G. W., & Hobbie, J. E. (1998). The character and bioactivity of dissolved organic matter at thaw and in the spring runoff waters of the arctic tundra North Slope, Alaska. *Journal of Geophysical Research Atmospheres*, 103(D22), 28939–28946. <https://doi.org/10.1029/98JD02650>
- Monteith, D. T., Stoddard, J. L., Evans, C. D., De Wit, H. A., Forsius, M., Høgåsen, T., Wilander, A., Skjelkvåle, B. L., Jeffries, D. S., Vuorenmaa, J., Keller, B., Kopéček, J., & Vesely, J. (2007). Dissolved organic carbon trends resulting from changes in atmospheric deposition chemistry. *Nature*, 450(7169), 537–540. <https://doi.org/10.1038/nature06316>
- O’Sullivan, D. W., Neale, P. J., Coffin, R. B., Boyd, T. J., & Osburn, C. L. (2005). Photochemical production of hydrogen peroxide and methylhydroperoxide in coastal waters. *Marine Chemistry*, 97(1–2), 14–33. <https://doi.org/10.1016/j.marchem.2005.04.003>
- Page, S. E., Kling, G. W., Sander, M., Harrold, K. H., Logan, J. R., McNeill, K., & Cory, R. M. (2013). Dark formation of hydroxyl radical in arctic soil and surface waters. *Environmental Science and Technology*, 47(22), 12860–12867. <https://doi.org/10.1021/es4033265>
- Page, S. E., Logan, J. R., Cory, R. M., & McNeill, K. (2014). Evidence for dissolved organic matter as the primary source and sink of photochemically produced hydroxyl radical in arctic surface waters. *Environmental Sciences: Processes and Impacts*, 16(4), 807–822. <https://doi.org/10.1039/c3em00596h>
- Pandey, D. R., Polik, C., & Cory, R. M. (2022). Controls on the photochemical production of hydrogen peroxide in Lake Erie. *Environmental Science: Processes and Impacts*, 24(11), 2108–2118. <https://doi.org/10.1039/d2em00327a>

- Petasne, R., & Zika, R. (1987). Fate of superoxide in coastal sea water. *Nature*, 325, 516–518.
- Powers, L. C., & Miller, W. L. (2014). Blending remote sensing data products to estimate photochemical production of hydrogen peroxide and superoxide in the surface ocean. *Environmental Sciences: Processes and Impacts*, 16(4), 792–806.
<https://doi.org/10.1039/c3em00617d>
- Samuel Lucas, and V, A, M. G., Environ Sci, H., Moffett, J. W., & Zika, R. G. (1987). Acknowledgments We thank John Koetz and Warren Bresler for performing the sampling Slivon for technical discussions and advice on manuscript revision. Literature Cited (1) National Research Council; Polycyclic Aromatic Hydro-carbons: Evaluation of Sources and Effects: A. Polynuclear Aromatic Hydrocarbons: Physical and Biological Reaction Kinetics of Hydrogen Peroxide with Copper and Iron in Seawater. In *J. Air Pollut. Control Assoc* (Vol. 21, Issue 2). Office of Research and Development.
<https://pubs.acs.org/sharingguidelines>
- Scully, N. M., McQueen, D. J., & Lean, D. R. S. (1996). Hydrogen peroxide formation: The interaction of ultraviolet radiation and dissolved organic carbon in lake waters along a 43–75°N gradient. *Limnology and Oceanography*, 41(3), 540–548.
<https://doi.org/10.4319/lo.1996.41.3.0540>
- Šmejkalová, T., Edwards, M. E., & Dash, J. (2016). Arctic lakes show strong decadal trend in earlier spring ice-out. *Scientific Reports*, 6. <https://doi.org/10.1038/srep38449>
- Stumm, W., & Lee1, G. F. (n.d.). *Oxygenation of Ferrous Iron*.
<https://pubs.acs.org/sharingguidelines>
- Trusiak, A., Treibergs, L. A., Kling, G. W., & Cory, R. M. (2018). The role of iron and reactive oxygen species in the production of CO₂ in arctic soil waters. *Geochimica et Cosmochimica Acta*, 224, 80–95. <https://doi.org/10.1016/j.gca.2017.12.022>
- Trusiak, A., Treibergs, L. A., Kling, G. W., & Cory, R. M. (2019). The controls of iron and oxygen on hydroxyl radical (\bullet OH) production in soils. *Soil Systems*, 3(1), 1–23.
<https://doi.org/10.3390/soilsystems3010001>
- Vermilyea, A. W., & Voelker, B. M. (2009). Photo-fenton reaction at near neutral pH. *Environmental Science and Technology*, 43(18), 6927–6933.
<https://doi.org/10.1021/es900721x>
- Walker, D. A., & Everett, K. R. (1991). Loess ecosystems of northern Alaska: Regional gradient and toposequence at Prudhoe Bay. *Ecological Monographs*, 61(4), 437–464.
<https://doi.org/10.2307/2937050>
- Ward, C. P., Bowen, J. C., Freeman, D. H., & Sharpless, C. M. (2021). Rapid and reproducible characterization of the wavelength dependence of aquatic photochemical reactions using light-emitting diodes. *Environmental Science and Technology Letters*, 8(5), 437–442.
<https://doi.org/10.1021/acs.estlett.1c00172>

- Ward, C. P., & Cory, R. M. (2015). Chemical composition of dissolved organic matter draining permafrost soils. *Geochimica et Cosmochimica Acta*, *167*, 63–79. <https://doi.org/10.1016/j.gca.2015.07.001>
- Ward, C. P., & Cory, R. M. (2016). Complete and Partial Photo-oxidation of Dissolved Organic Matter Draining Permafrost Soils. *Environmental Science and Technology*, *50*(7), 3545–3553. <https://doi.org/10.1021/acs.est.5b05354>
- Ward, C. P., Nalven, S. G., Crump, B. C., Kling, G. W., & Cory, R. M. (2017). Photochemical alteration of organic carbon draining permafrost soils shifts microbial metabolic pathways and stimulates respiration. *Nature Communications*, *8*(1). <https://doi.org/10.1038/s41467-017-00759-2>
- Weishaar, J. L., Aiken, G. R., Bergamaschi, B. A., Fram, M. S., Fujii, R., & Mopper, K. (2003). Evaluation of specific ultraviolet absorbance as an indicator of the chemical composition and reactivity of dissolved organic carbon. *Environmental Science and Technology*, *37*(20), 4702–4708. <https://doi.org/10.1021/es030360x>
- Whalen, S. C., & Cornwell, C. (1985). Nitrogen, Phosphorus, and Organic Carbon Cycling in an Arctic lake' For personal use only. In *Can. J. Fish. Aquat. Sci.* Downloaded from *cdnsiencepub.com* by UNIVERSITY OF MICHIGAN on (Vol. 42).
- Williamson, C. E., Overholt, E. P., Pilla, R. M., Leach, T. H., Brentrup, J. A., Knoll, L. B., Mette, E. M., & Moeller, R. E. (2015). Ecological consequences of long-term browning in lakes. *Scientific Reports*, *5*. <https://doi.org/10.1038/srep18666>
- Wolf, R., Andersen, T., Hessen, D. O., & Hylland, K. (2017). The influence of dissolved organic carbon and ultraviolet radiation on the genomic integrity of *Daphnia magna*. *Functional Ecology*, *31*(4), 848–855. <https://doi.org/10.1111/1365-2435.12730>
- Wolf, R., Thrane, J. E., Hessen, D. O., & Andersen, T. (2018). Modelling ROS formation in boreal lakes from interactions between dissolved organic matter and absorbed solar photon flux. *Water Research*, *132*, 331–339. <https://doi.org/10.1016/j.watres.2018.01.025>
- Wu, B., Liu, T., Wang, Y., Zhao, G., Chen, B., & Chu, C. (2021). High Sample Throughput LED Reactor for Facile Characterization of the Quantum Yield Spectrum of Photochemically Produced Reactive Intermediates. *Environmental Science and Technology*, *55*(23), 16204–16214. <https://doi.org/10.1021/acs.est.1c04608>
- Zepp, R. G., Faust, B. C., & Hoigné, J. (1992). Hydroxyl Radical Formation in Aqueous Reactions (pH 3-8) of Iron(II) with Hydrogen Peroxide: The Photo-Fenton Reaction. In *Environ. Sci. Technol* (Vol. 26). <https://pubs.acs.org/sharingguidelines>
- Zhang, Y., Del Vecchio, R., & Blough, N. V. (2012). Investigating the mechanism of hydrogen peroxide photoproduction by humic substances. *Environmental Science and Technology*, *46*(21), 11836–11843. <https://doi.org/10.1021/es3029582>

